

# Quantitative secretome analysis establishes the cell type-resolved mouse brain secretome

**Johanna Tüshaus<sup>12</sup>, Stephan A. Müller<sup>12</sup>, Evans Sioma Kataka<sup>4</sup>, Jan Zaucha<sup>4</sup>, Laura Sebastian Monasor<sup>1</sup>, Minhui Su<sup>15</sup>, Gökhan Güner<sup>12</sup>, Georg Jocher<sup>12</sup>, Sabina Tahirovic<sup>1</sup>, Dmitrij Frishman<sup>4</sup>, Mikael Simons<sup>135</sup> and Stefan F. Lichtenthaler<sup>123\*</sup>**

## Affiliations

<sup>1</sup>German Center for Neurodegenerative Diseases (DZNE), 81377 Munich, Germany

<sup>2</sup>Neuroproteomics, School of Medicine, Klinikum rechts der Isar, Technical University of Munich, 81675 Munich, Germany

<sup>3</sup>Munich Cluster for Systems Neurology (SyNergy), 81377 Munich, Germany

<sup>4</sup>Department of Bioinformatics, Wissenschaftszentrum Weihenstephan, Technical University of Munich, 85354 Freising, Germany

<sup>5</sup>Institute of Neuronal Cell Biology, Technical University Munich, 80802 Munich, Germany

\* To whom correspondence should be addressed: Stefan.Lichtenthaler@dzne.de

1    **Abstract**

2    **To understand how cells communicate in the nervous system, it is essential to define their  
3    secretome, which is challenging for primary cells because of large cell numbers being  
4    required. Here, we miniaturized secretome analysis by developing the high-performance  
5    secretome-protein-enrichment-with-click-sugars method (hiSPECS). To demonstrate its  
6    broad utility, hiSPECS was used to identify the secretory response of brain slices upon  
7    LPS-induced neuroinflammation and to establish the cell type-resolved mouse brain  
8    secretome resource using primary astrocytes, microglia, neurons and oligodendrocytes.  
9    This resource allowed mapping the cellular origin of CSF proteins and revealed that an  
10   unexpectedly high number of secreted proteins *in vitro* and *in vivo* are proteolytically-  
11   cleaved membrane protein ectodomains. Two examples are neuronally secreted ADAM22  
12   and CD200, which we identified as substrates of the Alzheimer-linked protease BACE1.  
13   hiSPECS and the brain secretome resource can be widely exploited to systematically study  
14   protein secretion, brain function and to identify cell type-specific biomarkers for CNS  
15   diseases.**

## 16 **Introduction**

17 Protein secretion is essential for inter-cellular communication and tissue homeostasis of  
18 multicellular organisms and has a central role in development, function, maintenance and  
19 inflammation of the nervous system. Proteins secreted from cells are referred to as the secretome  
20 and comprise secreted soluble proteins, such as insulin, granulins, APOE and extracellular matrix  
21 proteins (e.g. neurocan, fibronectin). The secretome also comprises the extracellular domains of  
22 membrane proteins, e.g. growth factors, cytokines, receptors and cell adhesion proteins (e.g.  
23 neuregulin, NCAM, N-cadherin), which are proteolytically generated by mostly membrane-bound  
24 proteases and secreted in a cellular process called ectodomain shedding (Lichtenthaler, Lemberg  
25 et al., 2018). However, it is largely unknown to what extent ectodomain shedding contributes to  
26 total protein secretion and how this differs between cell types in the brain.

27 Omics' approaches have generated large collections of mRNA and protein abundance data across  
28 the different cell types of the brain, e.g.(Sharma, Schmitt et al., 2015, Zhang, Chen et al., 2014).

29 In contrast, little is known about the proteins that are secreted from brain cells and whether – in  
30 parallel to their broad expression in different brain cell types – they are secreted from multiple  
31 brain cell types or instead are secreted in a cell type-specific manner *in vitro*, *ex vivo* (e.g.  
32 organotypic slice culture), *and in vivo*. Cerebrospinal fluid (CSF) constitutes an *in vivo* brain  
33 secretome and is an easily accessible body fluid widely used for studying brain (patho-)physiology  
34 and measuring and identifying disease biomarkers (Johnson, Dammer et al., 2020, Olsson,  
35 Lautner et al., 2016, Zetterberg & Bendlin, 2020), but it is largely unknown which cell type the CSF  
36 proteins are secreted from, because no systematic brain cell type-specific protein secretion  
37 studies are available.

38 Dysregulated protein secretion and shedding is linked to neurologic and psychiatric diseases,  
39 including neurodegeneration, e.g. APP, APOE, SORL1 and TREM2 in Alzheimer's disease (AD),  
40 or the prion protein (PRNP) in Prion disease (Lichtenthaler et al., 2018). Thus, identification and

41 quantification of secretomes does not only allow understanding of biological processes under  
42 physiological conditions, but also contributes to unravelling the molecular basis of diseases and  
43 identification of drug targets and biomarkers, such as shed TREM2 for AD (Ewers, Franzmeier et  
44 al., 2019, Schindler, Li et al., 2019, Suarez-Calvet, Araque Caballero et al., 2016).

45 Systematic identification and quantification of secretome proteins is commonly done using  
46 conditioned medium of a (primary) cell type and its analysis by mass spectrometry-based  
47 proteomics. A major challenge is the low concentration of secreted proteins within the conditioned  
48 medium(Schira-Heinen, Grube et al., 2019). Therefore, many studies concentrate medium from  
49 tens of millions of cells (Kleifeld, Doucet et al., 2010, Kleifeld, Doucet et al., 2011, Kuhn, Koroniak  
50 et al., 2012, Schlage, Kockmann et al., 2015, Wiita, Seaman et al., 2014). However, such numbers  
51 are often not available for primary cells, such as microglia, where on average one million cells  
52 may be purified from the brain of individual adult mice. Thus, miniaturized secretome analysis  
53 methods are required. A second major challenge is the large dynamic range of secretomes, in  
54 particular when cells are cultured in the presence of serum or serum-like supplements, which are  
55 highly abundant in proteins (most notably albumin), hampering the detection of endogenous, cell-  
56 derived secreted proteins, whose protein levels are typically orders of magnitude  
57 lower(Eichelbaum, Winter et al., 2012). Therefore, cells are often cultured under serum- and  
58 protein-free starvation conditions(Deshmukh, Cox et al., 2015, Kleifeld et al., 2010, Meissner,  
59 Scheltema et al., 2013), which, however, strongly alters secretome composition and may induce  
60 cell-death(Eichelbaum et al., 2012). An alternative approach, compatible with cell culture in the  
61 presence of serum or serum-like supplements, is to metabolically label the cell-derived, but not  
62 the exogenous serum proteins with analogs of methionine or sugars that are incorporated into the  
63 protein backbone or glycan structures, of newly synthesized cellular proteins, respectively  
64 (Eichelbaum et al., 2012, Kuhn et al., 2012). However, even these established methods still  
65 require extensive secretome fractionation, either at the protein or peptide level (Eichelbaum et al.,  
66 2012, Kuhn et al., 2012) and, thus result in laborious sample preparation, extensive mass

67 spectrometry measurement times and the requirement of large amounts of samples, which may  
68 not be available from primary cells or tissues.

69 Here, we developed the 'high-performance secretome protein enrichment with click sugars'  
70 (hiSPECS) method, which down-scales and speeds up secretome analysis and now allows  
71 secretome analysis of primary brain cells from single mice. We applied hiSPECS to determine the  
72 cell type-resolved mouse brain secretome, which establishes a resource for systematically  
73 studying protein secretion and shedding in the brain. Broad applicability of hiSPECS and the  
74 resource is demonstrated a) by gaining new insights into the extent of cell type-specific protein  
75 secretion and shedding, b) by identifying new substrates for the protease BACE1, a major drug  
76 target in AD, c) by determining the cellular origin of proteins in CSF and d) by revealing that LPS-  
77 induced inflammatory conditions in organotypic brain slices do not only lead to inflammatory  
78 protein secretion from microglia, but instead induce to a systemic secretory response from multiple  
79 cell types in brain slices.

80 **Results**

81 **Development of hiSPECS and benchmarking against SPECS**

82 To enable secretome analysis of primary brain cell types from single mice under physiological  
83 conditions (i.e. in the presence of serum-like supplements), we miniaturized the previously  
84 established SPECS method, which required 40 million cells per experiment (Kuhn et al., 2012).  
85 We introduced four major changes (Fig. 1A, see Supplementary Fig. 1A for a detailed comparison  
86 of hiSPECS versus SPECS). First, after labeling of cells with N-azido-mannosamine (ManNAz),  
87 an azido group-bearing sugar, secretome glycoproteins were enriched from the conditioned  
88 medium with lectin-based precipitation using concanavalin A (ConA). This strongly reduced  
89 albumin, which is not a glycoprotein (Supplementary Fig. 1B). Because the majority of soluble  
90 secreted proteins and most of the membrane proteins – which contribute to the secretome through  
91 shedding – are glycosylated (Kuhn, Colombo et al., 2016), hiSPECS can identify the major fraction  
92 of all secreted proteins. Second, we selectively captured the azido-glycoproteins by covalent  
93 binding to magnetic dibenzylcyclooctyne (DBCO)-alkyne-beads using copper-free click chemistry.  
94 This allowed stringent washing to reduce contaminating proteins. Third, on-bead digestion of the  
95 captured glycoproteins was performed to release tryptic peptides for mass spectrometry-based  
96 label-free protein quantification (LFQ). Fourth, mass spectrometry measurements were done on  
97 a Q-Exactive HF mass spectrometer using either data-dependent acquisition (DDA) or the more  
98 recently developed data-independent acquisition (DIA)(Bruderer, Bernhardt et al., 2015, Gillet,  
99 Navarro et al., 2012, Ludwig, Gillet et al., 2018)(Supplementary Fig.1C).

100 To benchmark hiSPECS against the previous SPECS protocol, we collected the secretome of  
101 primary murine neurons in the presence of a serum supplement as before (Kuhn et al., 2012), but  
102 used only one million neurons (40-fold fewer cells compared to SPECS). Despite this  
103 miniaturization, hiSPECS quantified on average 186% and 236% glycoproteins in DDA and DIA  
104 mode, respectively, compared to the previous SPECS dataset (Kuhn et al., 2012) (according to

105 UniProt and four previous glycoproteomic studies; Fig. 1B; Supplementary Fig.1D,E;  
106 Supplementary Table 1) (Fang, Wang et al., 2016, Joshi, Jorgensen et al., 2018, Liu, Zeng et al.,  
107 2017, Zielinska, Gnad et al., 2010). Furthermore, the DIA method provided 18% more quantified  
108 glycoproteins and 11% shed transmembrane proteins compared to DDA (Fig. 1C). Due to the  
109 superiority of DIA over DDA in secretome analysis we focused on hiSPECS DIA throughout the  
110 manuscript (Fig. 1D). 99.9% (2273/2276) of unique tryptic peptides identified from single-pass  
111 transmembrane proteins mapped to their known or predicted protein ectodomains. This is an  
112 important quality control which demonstrates that the secretome contains proteolytically shed  
113 transmembrane ectodomains and not full-length transmembrane proteins and that hiSPECS  
114 reliably identifies secretome-specific proteins (Fig. 1E).

115 The novel hiSPECS procedure does not require further protein or peptide fractionation. Thus,  
116 sample preparation time and mass spectrometer measurement time were both reduced 5-fold  
117 compared to previously required times (Fig. 1F). Importantly, hiSPECS also improved the  
118 reproducibility of protein LFQ among different biological replicates, which is reflected by an  
119 average Pearson correlation coefficient of 0.97 using hiSPECS in comparison to 0.84 with the  
120 previous procedure (Supplementary Fig.1F). Taken together, hiSPECS outperforms SPECS with  
121 regard to the required number of cells, sensitivity, reproducibility, protein coverage, sample  
122 preparation and mass spectrometry measurement time.

### 123 **Cell type-resolved mouse brain secretome resource**

124 Secreted soluble and shed proteins have key roles in signal transduction, but their cellular origin  
125 is often unclear as they may be expressed by multiple cell types. Thus, we used hiSPECS to  
126 establish a resource of the brain secretome in a cell type-resolved manner, focusing on the four  
127 major brain cell types – astrocytes, microglia, neurons and oligodendrocytes (Fig. 2A;  
128 Supplementary Table 2). One million primary cells of each cell type were prepared from individual  
129 mouse brains. For further analysis, we focused on proteins detected in the secretome of at least

130 five out of six biological replicates of at least one cell type. This yielded 995 protein groups in the  
131 secretome, with microglia having on average the largest (753) and astrocytes the smallest (503)  
132 number of protein groups (Fig. 2B). GO cellular compartment analysis revealed extracellular  
133 region to be the most enriched term underlining the quality of our secretome library  
134 (Supplementary Fig. 2A,B). An additional quality control measure was the enrichment of known  
135 cell type-specifically secreted marker proteins such as LINGO1, SEZ6 and L1CAM in the neuronal  
136 secretome (Supplementary Fig. 2C). Importantly, the secretome analysis identified 111 proteins  
137 (Fig. 2C) that were not detected in a previous proteomic study by Sharma *et al.* (Sharma *et al.*,  
138 2015) (Supplementary Table 3), that identified >10,000 proteins in the lysates of the same primary  
139 mouse brain cell types, which had been taken in culture as in our study (Supplementary Table 2).  
140 This includes soluble proteins (e.g. CPN1, TIMP1) and shed ectodomains (e.g. ADAM19, CRIM1,  
141 FRAS1) and even the protein GALNT18, which was assumed to be a pseudogene that is not  
142 expressed as a protein. Together, this demonstrates that secretome analysis is complementary to  
143 lysate proteomics in order to identify the whole proteome expressed in an organ.

144 Based on LFQ intensity values, the Pearson correlation coefficients between the six biological  
145 replicates of each cell type showed on average an excellent reproducibility with a value of 0.92  
146 (Fig. 2D). In strong contrast, the correlation between different cell types was dramatically lower  
147 (0.29 - 0.68), indicating prominent differences between the cell type-specific secretomes (Fig. 2D-  
148 F Supplementary Fig. 2D,3). In fact, about one third (322/995) of the secretome proteins were  
149 consistently detected (5/6 biological replicates) in the secretome of only one cell type and in fewer  
150 replicates or not at all within the other cell type secretomes (Fig. 2G), highlighting the unique cell  
151 type-characteristic secretome fingerprint of each cell type (Supplementary Table 4).

152 Cell type-specific protein secretion was visualized in a heat map (Fig. 3A, Supplementary Fig. 4A).  
153 Gene ontology analysis of the enriched secretome proteins revealed functional clusters  
154 corresponding to the known functions of the four individual cell types. For example, metabolic

155 process, gliogenesis and immune response was preferentially secreted from astrocytes (e.g.  
156 IGHM, CD14, LBP). Functional clusters autophagy and phagocytosis were secreted from  
157 microglia (e.g. TGFB1, MSTN, TREM2), in agreement with key microglial functions. Neuron-  
158 preferentially secreted proteins belonged to the neuron-specific categories axon guidance, trans-  
159 synaptic signaling and neurogenesis (e.g. NCAN, CHL1, SEZ6). Oligodendrocyte-specifically  
160 secreted proteins (e.g. OMG, ATRN, TNFRSF21) fell into categories lipid metabolic process and  
161 myelination, in agreement with the role of oligodendrocytes in myelin sheet formation. This  
162 demonstrates that cell function can be obtained by a cell's secretome (Fig. 3A, Supplementary  
163 Fig.4B).

164 Secreted proteins may act as soluble cues to signal to other cells. To unravel the inter-cellular  
165 communication between secreted proteins and transmembrane proteins acting as potential  
166 binding partners/receptors, we mapped known interaction partners (from UniProt and BioGRID  
167 (Chatr-Aryamontri, Breitkreutz et al., 2015, UniProt Consortium, 2018)), but now in a cell type-  
168 resolved manner (Fig. 3B and Supplementary Table 5). Besides known cell type-specific  
169 interactions, such as between neuronally secreted CD200 and its microglia-expressed receptor  
170 CD200R1 (Yi, Zhang et al., 2016), we also detected new cell type-specific interactions, e.g.  
171 between ADIPOQ (adiponectin) and CDH13. Adiponectin is a soluble anti-inflammatory adipokine  
172 with key functions in metabolism, but also in neurogenesis and neurodegeneration (Lee, Cheng  
173 et al., 2019). Although adiponectin is thought to be secreted exclusively from adipocytes and  
174 assumed to reach the brain by crossing the blood-brain-barrier, our resource and the cell type-  
175 resolved interaction map reveal that adiponectin can also be produced and secreted from brain  
176 cells (oligodendrocytes). The binding to one of its receptors, cadherin13 (neurons), establishes a  
177 new interaction between oligodendrocytes and neurons, which may have an important role in  
178 controlling the multiple, but not yet well understood, adiponectin functions in the brain.

179 Besides pronounced cell type-specific protein secretion, another key insight obtained from our  
180 secretome resource is that ectodomain shedding of membrane proteins strongly contributes to the  
181 composition of the secretome (43%, 242/568 glycoproteins according to UniProt). The extent  
182 differed between the major mouse brain cell types (Fig. 3C) and became even more evident when  
183 focusing on the cell type-specifically secreted proteins. More than two thirds (71%, 74/104) of the  
184 neuron-specifically secreted proteins were shed ectodomains (Fig. 3D), i.e. proteins annotated as  
185 transmembrane or GPI-anchored proteins, of which we almost only (99.9%) identified peptides  
186 from the ectodomain (Fig. 1E). The neuronally shed ectodomains contain numerous trans-  
187 synaptic signaling and cell adhesion proteins (NRXN1, SEZ6, CNTNAP4) indicating that shedding  
188 is an important mechanism for controlling signaling and synaptic connectivity in the nervous  
189 system. In contrast to neurons, shedding appeared quantitatively less important in astrocytes,  
190 where only 21% (9/43) of the cell type-specifically secreted proteins were shed ectodomains (Fig.  
191 3D). In contrast, soluble secreted proteins are particularly relevant for astrocytes and microglia  
192 where they constituted 70% (30/43) and 62% (38/61) of the secretome proteins, respectively, and  
193 contain numerous soluble proteins with functions in inflammation, e.g. complement proteins and  
194 TIMP1 (astrocytes) and GRN, MMP9, PLAU, TGFB1 (microglia). Importantly, several soluble  
195 secreted proteins were expressed at similar levels in different brain cell types, but predominantly  
196 secreted from only one, suggesting that cell type-specific protein secretion may be an important  
197 mechanism to control brain inflammation. Examples are the astrocyte-secreted complement factor  
198 B and the microglia-secreted LTBP4 (Supplementary Table 4).

#### 199 **Mechanisms of cell type-specific protein secretion**

200 Abundance levels in the lysate of the majority of proteins are similar among astrocytes, microglia,  
201 neurons and oligodendrocytes, with only around 15% of the proteins present in a cell type-specific  
202 manner (Sharma et al., 2015). In clear contrast, we observed that in the secretome of the same  
203 cell types, nearly half (420/995 proteins) of the secreted proteins were secreted in a cell type-  
204 specific manner (>5-fold enriched in one secretome compared to all three others or consistently

205 detected in the secretome of only one cell type) (Supplementary Table 4), suggesting that cell  
206 type-specific protein secretion strongly contributes to functional differences between the four brain  
207 cell types.

208 An obvious mechanism explaining cell type-specific protein secretion is cell type-specific  
209 expression of the secreted soluble or shed proteins. Unexpectedly, however, a correlation with  
210 cell type-specific protein abundance in the same cell types (Sharma et al., 2015) was observed  
211 for only 20-30% of the cell type-specifically secreted proteins (Fig. 4A), including the TGF $\beta$   
212 coreceptor CD109 from astrocytes, the inflammatory proteins GRN, BIN2, TGF $\beta$ 1 from microglia,  
213 the cell adhesion proteins CD200, L1CAM, and the bioactive peptide secretogranin (CHGB) from  
214 neurons and CSPG4, PDGFR $\alpha$ , OMG and BCHE from oligodendrocytes (examples shown in Fig.  
215 4A,B and Supplementary Fig.5). This demonstrates that cell type-specific expression is only a  
216 minor or only one of several mechanisms controlling cell type-specific protein secretion and  
217 shedding. In fact, the vast majority of cell type-specifically secreted proteins were equally  
218 expressed in two or more cell types (Fig. 4A).

219 Because we observed that shedding contributes significantly to protein secretion, particularly in  
220 neurons, we considered the possibility that cell type-specific protein shedding may mechanistically  
221 also depend on cell type-specific expression of the contributing shedding protease. For example,  
222 the Alzheimer's disease-linked protease  $\beta$ -site APP cleaving enzyme (BACE1)(Vassar, Bennett  
223 et al., 1999, Yan, Bienkowski et al., 1999), which has fundamental functions in the brain, is highly  
224 expressed in neurons, but not in astrocytes, microglia or oligodendrocytes (Voytyuk, Mueller et  
225 al., 2018). Consistent with our hypothesis, several known BACE1 substrates (APLP1, CACHD1,  
226 PCDH20 and SEZ6L) which are broadly expressed, were specifically shed from neurons  
227 (examples shown in Fig. 4A,B and Supplementary Fig.5). To investigate whether additional  
228 proteins in our secretome resource may be shed by BACE1 in a cell type-specific manner, primary  
229 neurons were treated with the established BACE1 inhibitor C3 (Stachel, Coburn et al., 2004)(Fig.

230 5A; Supplementary Table 6), followed by hiSPECS. This yielded 29 membrane proteins with  
231 reduced ectodomain levels in the secretome (Fig. 5B and Supplementary Fig.6A,B;  
232 Supplementary Table 7), which were scored as BACE1 substrate candidates. Besides known  
233 substrates, hiSPECS identified additional BACE1 substrate candidates (ADAM22, CD200,  
234 CXADR, and IL6ST) in neurons (Fig. 5B).

235 ADAM22, which is a new BACE1 substrate candidate, and CD200, which was previously  
236 suggested as a BACE1 substrate candidate in a peripheral cell line (Stutzer, Selevsek et al.,  
237 2013), were further validated as neuronal BACE1 substrates by Western blots and ELISA assays  
238 (Fig. 5C-E). For CD200 we also detected a semi-tryptic peptide in the conditioned medium of  
239 neurons and in a previous proteomic data set (Pigoni, Wanngren et al., 2016) of murine  
240 cerebrospinal fluid (CSF) (Fig. 5F,G), but not when BACE1 was inhibited in the neurons or in the  
241 CSF of mice lacking BACE1 and its homolog BACE2 (Pigoni et al., 2016). As this semi-tryptic  
242 peptide derives from the juxtamembrane domain of CD200 where BACE1 typically cleaves its  
243 substrates, this peptide likely represents the cleavage site of BACE1 in CD200 (Fig. 5G). The  
244 validation of CD200 as a new *in vivo* BACE1 substrate demonstrates the power of hiSPECS to  
245 unravel the substrate repertoire of transmembrane proteases and reveals that cell type-specific  
246 expression of an ectodomain shedding protease is an important mechanism controlling the cell  
247 type-specific secretion/shedding of proteins.

248 Taken together, cell type-specific protein secretion and shedding is minimally dependent on cell  
249 type-specific protein expression of the secreted protein. Instead, cell type-specific expression of  
250 shedding regulators and other mechanisms to be discovered have an important role in determining  
251 cell type-specific protein secretion.

## 252 **Cell type-specific origin of CSF proteins**

253 Cerebrospinal fluid (CSF) is the body fluid in direct contact with the brain and serves as an *in vivo*  
254 secretome. It is widely used for basic and preclinical research as well as clinical applications.

255 However, a major limitation of CSF studies is that changes in CSF composition induced by disease  
256 or treatments often cannot be traced back to the cell type of origin, because most CSF proteins  
257 are expressed in multiple cell types (Sharma et al., 2015). To overcome this limitation, we applied  
258 the cell type-resolved brain secretome resource derived from the four most abundant brain cell  
259 types to determine the likely cellular origin of secreted glycoproteins in CSF (Supplementary Table  
260 8).

261 In CSF from individual wild-type mice, 984 protein groups were identified with DIA in at least 3 out  
262 of 4 biological replicates (Fig. 6A), which represents higher coverage than in previous mouse CSF  
263 studies (Dislich, Wohlrab et al., 2015, Pigoni et al., 2016) and underlines the superiority of DIA  
264 over DDA in samples with low protein concentration. Proteins were grouped according to their  
265  $\log_{10}$  DIA LFQ intensities (as a rough estimate of protein abundance) into quartiles and analyzed  
266 according to their UniProt annotations for membrane, secreted, and cytoplasm (Fig. 5A). Soluble  
267 secreted proteins, such as APOE, were more abundant in the 1<sup>st</sup> quartile, whereas the shed  
268 ectodomains, e.g. of CD200 and ADAM22, were the largest group of proteins in the 3<sup>rd</sup> and 4<sup>th</sup>  
269 quartile, indicating their lower abundance in CSF as compared to the soluble secreted proteins.

270 Among the 476 CSF proteins annotated as glycoproteins (UniProt), 311 (65%) were also detected  
271 in the hiSPECs secretome resource and were mapped to the corresponding cell type (Fig. 6B).  
272 The most abundant glycoproteins of each cell type (top 25) revealed also high coverage in the  
273 CSF up to 76% of the top 25 neuronal proteins (Supplementary Fig. 7A). In general, proteins of  
274 neuronal origin represented the largest class of CSF glycoproteins and this was independent of  
275 their abundance (Fig. 6B,C). Given that astrocytes and oligodendrocytes outnumber neurons by  
276 far in the brain, this demonstrates that neurons disproportionately contribute to the CSF proteome.  
277 This prominent role of neurons is also reflected when focusing on the 420 cell type-specifically  
278 secreted proteins of our brain secretome resource. 123 of these proteins were also found in murine  
279 CSF (Fig. 6D). The majority in each quartile were proteins of neuronal origin. Similar to the proteins

280 secreted from the four major brain cell types *in vitro*, the largest amount of the cell type-specifically  
281 secreted proteins detected in CSF are expressed in multiple cell types, but only secreted from one  
282 (Supplementary Table 4). This includes BACE1 substrates, such as SEZ6L and CACHD1, in  
283 agreement with BACE1 being expressed in neurons, but not in other brain cell types (Voytyuk et  
284 al., 2018). Thus, cell type-specific protein expression as well as cell type-specific protease  
285 expression and potentially additional mechanisms govern cell type-specific protein secretion, both  
286 *in vitro* (hiSPECS resource) and *in vivo* (CSF).

287 Several of the detected murine CSF proteins have human homologs linked to brain diseases  
288 (DisGeNET database (Pinero, Bravo et al., 2017)) and may serve as potential biomarkers. We  
289 mapped these proteins to their likely cell type of origin (Fig. 6E). Numerous proteins were  
290 specifically secreted from only one cell type, such as APP from neurons or granulin (GRN) from  
291 microglia, which have major roles in neurodegenerative diseases (Chitramuthu, Bennett et al.,  
292 2017, O'Brien & Wong, 2011). Thus, assigning the disease-related CSF/secretome proteins to  
293 one specific cell type offers an excellent opportunity to study the relevant cell type with regard to  
294 its contribution to disease pathogenesis. One example is the protein SORL1, which is genetically  
295 linked to Alzheimer's disease (Yin, Yu et al., 2015). Although SORL1 is similarly expressed in all  
296 four major brain cell types, it was specifically released from neurons in the hiSPECS resource  
297 (Supplementary Table 4), indicating that pathology-linked changes in CSF SORL1 levels are likely  
298 to predominantly result from neurons.

299 Large-scale proteomic analyses of AD brain tissue and CSF (Bai, Wang et al., 2020, Johnson et  
300 al., 2020) continue to reveal more AD-linked proteins, such as increased CD44 in the CSF of AD  
301 patients (Johnson et al., 2020). Our resource demonstrates that CD44 is predominantly secreted  
302 from oligodendrocytes among the mouse brain cells, although having similar protein abundance  
303 in different brain cell types (Sharma et al., 2015)(Supplementary Fig.5). This data suggest to focus  
304 on oligodendrocytes for future studies determining how increased CD44 levels are mechanistically

305 linked to AD pathophysiology. Taken together, the hiSPECS resource enables systematic  
306 assignment of CSF glycoproteins to the specific cell type of origin, which offers multiple  
307 opportunities to study CNS diseases.

308 **Cell type-resolved brain tissue-secretome**

309 Next, we tested whether hiSPECS and the brain secretome resource can be used to determine  
310 the cell type-resolved secretome of brain tissue. We used organotypic cortico-hippocampal brain  
311 slices (Supplementary Table 9), an ex-vivo model of the brain (Daria, Colombo et al., 2017) that  
312 preserves the complex network of the diverse brain cell types. Despite the high amounts (25%) of  
313 serum proteins, 249 protein groups were identified in at least 5 of 6 biological replicates using  
314 hiSPECS DIA (Fig. 7A), demonstrating that hiSPECS is applicable for ex vivo brain tissue.  
315 Proteins were grouped according to their  $\log_{10}$  abundance into quartiles (Fig. 7B). Similar to CSF,  
316 the majority of the more abundant proteins in the 1<sup>st</sup> and 2<sup>nd</sup> quartile were soluble proteins,  
317 whereas the shed transmembrane protein ectodomains were in the 3<sup>rd</sup> and 4<sup>th</sup> quartile, indicating  
318 their lower protein abundance compared to the soluble secreted proteins. 89% of the proteins  
319 detected in the slice culture secretome were also detected in the hiSPECS secretome library of  
320 the different brain cell types, which allows tracing them back to their cellular origin (Fig 7B). The  
321 cell-type resolved tissue-secretome revealed on average the highest contribution of microglia  
322 (74%), followed by astrocytes (72.8%), oligodendrocytes (68.5%) and neurons (66.5%).  
323 Interestingly, in quartile one, which resembles the most abundant proteins, oligodendrocytes are  
324 the most prominent with 85%. In addition, numerous cell type-specifically secreted proteins were  
325 identified (Fig. 7C).

326 As a final application of the brain secretome resource, we treated brain slices for 6 h with the  
327 strong inflammatory stimulus lipopolysaccharide (LPS), which serves as a model for acute  
328 neuroinflammation. Conditioned medium was analyzed using hiSPECS DIA. LPS strongly  
329 changed the brain slice secretome. Secretion of several proteins (marked in red) known to be

330 LPS-responsive in macrophages(Meissner et al., 2013), such as H2-D1, CD14, or IL12B, were  
331 strongly upregulated (up to 250-fold) (Fig. 7D, Supplementary Table 9). Likewise, secretion of  
332 several proteins not known to be secreted in an LPS-dependent manner, such as BCAN, CHI3L1  
333 and the complement receptor C1RA, were strongly upregulated. Among the 107 significantly  
334 regulated proteins ( $p<0.05$ ) 50% and 26% are annotated as secreted proteins or single pass  
335 transmembrane proteins, respectively (Fig. 7E). Comparison of the brain slice secretome data to  
336 the secretome resource revealed that several proteins were secreted cell type-specifically, such  
337 as SORT1 and CHL1 by neurons and ENPP5 and ADIPOQ by oligodendrocytes (Fig. 7F). This  
338 demonstrates that not only immune cells responded with changes in their secretome to the  
339 inflammation cue, but instead indicates a systemic inflammatory response of multiple cell types.  
340 Moreover, this experiment suggests that systematic, proteome-wide secretome analysis of *ex vivo*  
341 brain slices is well suited to identify proteins and cell types contributing to neuroinflammation and  
342 potentially neurodegeneration.

343

## 344 **Discussion**

345 Omics' approaches have generated large collections of mRNA and protein abundance data across  
346 different cell types, including microglia and neurons, but we know very little about the molecules  
347 that are secreted from cells. This information is essential for our understanding of basic  
348 mechanisms of protein secretion, cell-cell communication within organs, particularly within the  
349 brain, and for identification of suitable biomarkers for brain processes in health and disease, such  
350 as APOE and TREM2 in AD(Huang, Zhou et al., 2019, Wolfe, Fitz et al., 2018).

351 Our development of the novel method hiSPECS miniaturizes mass spectrometry-based  
352 secretome analysis and enables secretome analysis of primary cell types, including the lower  
353 abundant ones in the brain. Importantly, hiSPECS allows culturing cells in the presence of serum  
354 or physiological cell culture supplements, whereas most previous secretome studies were

355 restricted to serum- and even protein-free culture conditions, which is not feasible with many  
356 primary cell types. Besides its broad applicability to primary cells, we demonstrate that hiSPECS  
357 can also be applied to brain tissue *ex vivo*, which is widely used in neuroscience. The streamlined  
358 hiSPECS workflow also facilitates a broad applicability in laboratories without proteomic expertise.  
359 The strongly reduced mass spectrometer measurement time enables cost-effective, single-shot  
360 proteomic analysis of the samples.

361 With hiSPECS we established the cell type-resolved secretome resource of the four major cell  
362 types in the brain and its application to map the putative cell type-specific origin of CSF proteins  
363 (*in vivo* secretome) and proteins secreted from brain slices (*ex vivo* secretome). This approach  
364 provided fundamental new biological insights. First, ectodomain shedding is a major mechanism  
365 contributing to the protein composition of the secretome and quantitatively differs between brain  
366 cell types. Second, shed proteins *in vitro* (primary cells), *ex vivo* (brain slices) and *in vivo* (CSF)  
367 have a generally lower abundance in the secretome than secreted soluble proteins. This is  
368 consistent with the function of the shedding process as a regulatory mechanism, which releases  
369 bioactive membrane protein ectodomains on demand into the secretome, as seen with  
370 cytokines(Lichtenthaler et al., 2018). Thus, shedding provides an additional layer of control for the  
371 composition of the secretome that goes beyond constitutive protein secretion. Third, protein  
372 secretion is a highly cell type-specific process in the nervous system. This is surprising because  
373 we found that more than 73% of the cell type-specifically secreted proteins were expressed in  
374 more than one cell type, demonstrating that cells do not simply control secretion through cell type-  
375 specific expression of the secreted protein, but instead must have acquired additional mechanisms  
376 to control cell type-specific protein secretion, which are not yet well understood. Our resource  
377 provides insights into the underlying mechanisms. One example is the cell type-specific  
378 expression of a shedding protease, such as BACE1 in neurons. Ectodomain shedding happens  
379 for more than 1,000 membrane proteins (Lichtenthaler et al., 2018), but in most cases, the  
380 contributing protease is not known. Thus, it is likely that shedding proteases other than BACE1

381 are also expressed in a cell type-specific manner, and thus contribute to cell type-specific protein  
382 shedding in the brain.

383 While additional mechanisms underlying cell type-specific protein secretion remain to be  
384 elucidated, protein transport through the secretory pathway, which is a prerequisite for protein  
385 secretion or shedding, is a potential mechanism of regulation. In fact, some soluble proteins  
386 require CAB45 for their exit from the trans-Golgi network, whereas other proteins do not(Blank &  
387 von Blume, 2017). Likewise, some transmembrane proteins require specific transport helpers for  
388 trafficking through the secretory pathway such as IRHOM1/2 for ADAM17 and Cornichon for  
389 transforming growth factor(Dancourt & Barlowe, 2010, Lichtenthaler, 2012). Thus, it appears  
390 possible that transport-selective proteins may be preferentially expressed in some brain cell types  
391 and consequently allow for a cell type-specific secretion or shedding of their cargo proteins.  
392 hiSPECS is an excellent method to address these fascinating questions regarding the complex  
393 mechanisms controlling protein secretion in the nervous system.

394 The secretome of the four major brain cell types and the *ex vivo* tissue identified here represents  
395 a snapshot of the total brain secretome and more secreted proteins are known or likely to exist.  
396 These include non-glycosylated secreted proteins which are not captured with hiSPECS as well  
397 as proteins secreted in a time-dependent manner such as during development or aging. For  
398 example, it is known that microglia can partially change their expression profile when taken into  
399 the culture, which may consequently affect the secretome (Gosselin, Skola et al., 2017).  
400 Additionally, the secretome may change upon cell stimulation, such as during neuronal activity or  
401 inflammation or when different cell types are cocultured or taken into three-dimensional culture  
402 systems (Stiess, Wegehingel et al., 2015). Additional proteins may be selectively secreted from  
403 lower abundant brain cell types, such as pericytes.

404 Taken together, hiSPECS and the cell type-resolved mouse brain secretome resource are  
405 important new tools for many areas in neuroscience, from mechanisms of protein secretion and

406 signal transduction between brain cells *in vitro*, *ex vivo* (brain slices) and *in vivo* (CSF) to functional  
407 analysis of nervous system proteins (identification of protease substrates) and cell type-specific  
408 biomarker determination in CSF (e.g. CD44) with high relevance to psychiatric, neurological and  
409 neurodegenerative diseases.

410

## 411 **Acknowledgement**

412 We thank Felix Meissner and Jürgen Cox for helpful comments on this manuscript, and Anna  
413 Daria for support with the *ex vivo* model. This work was supported by the Deutsche  
414 Forschungsgemeinschaft (German Research Foundation) within the framework of the Munich  
415 Cluster for Systems Neurology (EXC 2145 SyNergy, project ID 390857198) and the BMBF through  
416 project CLINSPECT-M and JPND PMG-AD. JT was supported by a Boehringer Ingelheim Fonds  
417 (BIF) PhD fellowship. Funds have been provided to ST by the Alzheimer Forschung Initiative e.V.  
418 (project number 18014)

## 419 **Author Contributions**

420 JT, SAM, SFL designed the experiments and prepared the manuscript. JT, SAM performed the  
421 proteomic analysis of all samples. JT, SAM analyzed the data with bioinformatics input from ESK,  
422 JZ, DF and GG. LSM, ST provided primary microglia and cortico-hippocampal brain slices. MS  
423 and MS provided primary oligodendrocyte culture and MS also gave conceptual advice.

## 424 **Declaration of Interests**

425 The authors declare no competing interests.

426

427 **References**

428 Bai B, Wang X, Li Y, Chen PC, Yu K, Dey KK, Yarbro JM, Han X, Lutz BM, Rao S, Jiao Y, Sifford JM, Han J, Wang  
429 M, Tan H, Shaw TI, Cho JH, Zhou S, Wang H, Niu M et al. (2020) Deep Multilayer Brain Proteomics  
430 Identifies Molecular Networks in Alzheimer's Disease Progression. *Neuron* 105: 975-991.e7

431 Blank B, von Blume J (2017) Cab45-Unraveling key features of a novel secretory cargo sorter at the trans-  
432 Golgi network. *European journal of cell biology* 96: 383-390

433 Bruderer R, Bernhardt OM, Gandhi T, Miladinović SM, Cheng L-Y, Messner S, Ehrenberger T, Zanotelli V,  
434 Butscheid Y, Escher C, Vitek O, Rinner O, Reiter L (2015) Extending the limits of quantitative proteome  
435 profiling with data-independent acquisition and application to acetaminophen-treated three-  
436 dimensional liver microtissues. *Molecular & cellular proteomics : MCP* 14: 1400-1410

437 Chatr-Aryamontri A, Breitkreutz BJ, Oughtred R, Boucher L, Heinicke S, Chen D, Stark C, Breitkreutz A, Kolas  
438 N, O'Donnell L, Reguly T, Nixon J, Ramage L, Winter A, Sellam A, Chang C, Hirschman J, Theesfeld C,  
439 Rust J, Livstone MS et al. (2015) The BioGRID interaction database: 2015 update. *Nucleic acids  
440 research* 43: D470-8

441 Chitramuthu BP, Bennett HPJ, Bateman A (2017) Programulin: a new avenue towards the understanding  
442 and treatment of neurodegenerative disease. *Brain* 140: 3081-3104

443 Dancourt J, Barlowe C (2010) Protein sorting receptors in the early secretory pathway. *Annual review of  
444 biochemistry* 79: 777-802

445 Daria A, Colombo A, Llovera G, Hampel H, Willem M, Liesz A, Haass C, Tahirovic S (2017) Young microglia  
446 restore amyloid plaque clearance of aged microglia. *The EMBO journal* 36: 583-603

447 Deshmukh AS, Cox J, Jensen LJ, Meissner F, Mann M (2015) Secretome Analysis of Lipid-Induced Insulin  
448 Resistance in Skeletal Muscle Cells by a Combined Experimental and Bioinformatics Workflow. *Journal  
449 of proteome research* 14: 4885-95

450 Diaz-Papkovich A, Anderson-Trocme L, Ben-Eghan C, Gravel S (2019) UMAP reveals cryptic population  
451 structure and phenotype heterogeneity in large genomic cohorts. *PLoS genetics* 15: e1008432

452 Dislich B, Wohlrab F, Bachhuber T, Muller SA, Kuhn PH, Hogl S, Meyer-Luehmann M, Lichtenthaler SF  
453 (2015) Label-free Quantitative Proteomics of Mouse Cerebrospinal Fluid Detects beta-Site APP  
454 Cleaving Enzyme (BACE1) Protease Substrates In Vivo. *Molecular & cellular proteomics : MCP* 14:  
455 2550-63

456 Eichelbaum K, Winter M, Berriel Diaz M, Herzig S, Krijgsveld J (2012) Selective enrichment of newly  
457 synthesized proteins for quantitative secretome analysis. *Nature biotechnology* 30: 984-90

458 Ewers M, Franzmeier N, Suarez-Calvet M, Morenas-Rodriguez E, Caballero MAA, Kleinberger G, Piccio L,  
459 Cruchaga C, Deming Y, Dichgans M, Trojanowski JQ, Shaw LM, Weiner MW, Haass C (2019) Increased  
460 soluble TREM2 in cerebrospinal fluid is associated with reduced cognitive and clinical decline in  
461 Alzheimer's disease. *Science translational medicine* 11

462 Fang P, Wang XJ, Xue Y, Liu MQ, Zeng WF, Zhang Y, Zhang L, Gao X, Yan GQ, Yao J, Shen HL, Yang PY (2016)  
463 In-depth mapping of the mouse brain N-glycoproteome reveals widespread N-glycosylation of diverse  
464 brain proteins. *Oncotarget* 7: 38796-38809

465 Gillet LC, Navarro P, Tate S, Rost H, Selevsek N, Reiter L, Bonner R, Aebersold R (2012) Targeted data  
466 extraction of the MS/MS spectra generated by data-independent acquisition: a new concept for  
467 consistent and accurate proteome analysis. *Molecular & cellular proteomics : MCP* 11: O111.016717

468 Gosselin D, Skola D, Coufal NG, Holtman IR, Schlachetzki JCM, Sajti E, Jaeger BN, O'Connor C, Fitzpatrick C,  
469 Pasillas MP, Pena M, Adair A, Gonda DD, Levy ML, Ransohoff RM, Gage FH, Glass CK (2017) An  
470 environment-dependent transcriptional network specifies human microglia identity. *Science (New  
471 York, NY)* 356

472 Huang da W, Sherman BT, Lempicki RA (2009a) Bioinformatics enrichment tools: paths toward the  
473 comprehensive functional analysis of large gene lists. *Nucleic acids research* 37: 1-13

474 Huang da W, Sherman BT, Lempicki RA (2009b) Systematic and integrative analysis of large gene lists using  
475 DAVID bioinformatics resources. *Nature protocols* 4: 44-57

476 Huang YA, Zhou B, Nabet AM, Wernig M, Sudhof TC (2019) Differential Signaling Mediated by ApoE2,  
477 ApoE3, and ApoE4 in Human Neurons Parallels Alzheimer's Disease Risk. *J Neurosci* 39: 7408-7427

478 Johnson ECB, Dammer EB, Duong DM, Ping L, Zhou M, Yin L, Higginbotham LA, Guajardo A, White B,  
479 Troncoso JC, Thambisetty M, Montine TJ, Lee EB, Trojanowski JQ, Beach TG, Reiman EM, Haroutunian  
480 V, Wang M, Schadt E, Zhang B et al. (2020) Large-scale proteomic analysis of Alzheimer's disease brain  
481 and cerebrospinal fluid reveals early changes in energy metabolism associated with microglia and  
482 astrocyte activation. *Nature Medicine*

483 Joshi HJ, Jorgensen A, Schjoldager KT, Halim A, Dworkin LA, Steentoft C, Wandall HH, Clausen H,  
484 Vakhrushev SY (2018) GlycoDomainViewer: a bioinformatics tool for contextual exploration of  
485 glycoproteomes. *Glycobiology* 28: 131-136

486 Kammers K, Cole RN, Tiengwe C, Ruczinski I (2015) Detecting Significant Changes in Protein Abundance.  
487 *EuPA open proteomics* 7: 11-19

488 Kleifeld O, Doucet A, auf dem Keller U, Prudova A, Schilling O, Kainthan RK, Starr AE, Foster LJ,  
489 Kizhakkedathu JN, Overall CM (2010) Isotopic labeling of terminal amines in complex samples  
490 identifies protein N-termini and protease cleavage products. *Nature biotechnology* 28: 281-8

491 Kleifeld O, Doucet A, Prudova A, auf dem Keller U, Gioia M, Kizhakkedathu JN, Overall CM (2011) Identifying  
492 and quantifying proteolytic events and the natural N terminome by terminal amine isotopic labeling  
493 of substrates. *Nature protocols* 6: 1578-611

494 Kuhn PH, Colombo AV, Schusser B, Dreymueller D, Wetzel S, Schepers U, Herber J, Ludwig A, Kremmer E,  
495 Montag D, Muller U, Schweizer M, Saftig P, Bräse S, Lichtenthaler SF (2016) Systematic substrate  
496 identification indicates a central role for the metalloprotease ADAM10 in axon targeting and synapse  
497 function. *eLife* 5

498 Kuhn PH, Koroniak K, Hogl S, Colombo A, Zeitschel U, Willem M, Volbracht C, Schepers U, Imhof A,  
499 Hoffmeister A, Haass C, Rossner S, Bräse S, Lichtenthaler SF (2012) Secretome protein enrichment  
500 identifies physiological BACE1 protease substrates in neurons. *The EMBO journal* 31: 3157-68

501 Lee TH, Cheng KK, Hoo RL, Siu PM, Yau SY (2019) The Novel Perspectives of Adipokines on Brain Health.  
502 *International journal of molecular sciences* 20

503 Lichtenthaler SF (2012) Cell biology. Sheddase gets guidance. *Science (New York, NY)* 335: 179-80

504 Lichtenthaler SF, Lemberg MK, Flührer R (2018) Proteolytic ectodomain shedding of membrane proteins  
505 in mammals-hardware, concepts, and recent developments. *The EMBO journal* 37

506 Liu MQ, Zeng WF, Fang P, Cao WQ, Liu C, Yan GQ, Zhang Y, Peng C, Wu JQ, Zhang XJ, Tu HJ, Chi H, Sun RX,  
507 Cao Y, Dong MQ, Jiang BY, Huang JM, Shen HL, Wong CCL, He SM et al. (2017) pGlyco 2.0 enables  
508 precision N-glycoproteomics with comprehensive quality control and one-step mass spectrometry for  
509 intact glycopeptide identification. *Nature communications* 8: 438

510 Ludwig C, Gillet L, Rosenberger G, Amon S, Collins BC, Aebersold R (2018) Data-independent acquisition-  
511 based SWATH-MS for quantitative proteomics: a tutorial. *Molecular systems biology* 14: e8126

512 Meissner F, Scheltema RA, Mollenkopf HJ, Mann M (2013) Direct proteomic quantification of the  
513 secretome of activated immune cells. *Science (New York, NY)* 340: 475-8

514 O'Brien RJ, Wong PC (2011) Amyloid precursor protein processing and Alzheimer's disease. *Annu Rev  
515 Neurosci* 34: 185-204

516 Olsson B, Lautner R, Andreasson U, Ohrfelt A, Portelius E, Bjerke M, Holtta M, Rosen C, Olsson C, Strobel  
517 G, Wu E, Dakin K, Petzold M, Blennow K, Zetterberg H (2016) CSF and blood biomarkers for the  
518 diagnosis of Alzheimer's disease: a systematic review and meta-analysis. *The Lancet Neurology* 15:  
519 673-684

520 Pignoni M, Wanngren J, Kuhn PH, Munro KM, Gunnersen JM, Takeshima H, Feederle R, Voytyuk I, De  
521 Strooper B, Levasseur MD, Hrupka BJ, Muller SA, Lichtenthaler SF (2016) Seizure protein 6 and its

522 homolog seizure 6-like protein are physiological substrates of BACE1 in neurons. *Molecular*  
523 *neurodegeneration* 11: 67

524 Pinero J, Bravo A, Queralt-Rosinach N, Gutierrez-Sacristan A, Deu-Pons J, Centeno E, Garcia-Garcia J, Sanz  
525 F, Furlong LI (2017) DisGeNET: a comprehensive platform integrating information on human disease-  
526 associated genes and variants. *Nucleic acids research* 45: D833-d839

527 Rappaport J, Ishihama Y, Mann M (2003) Stop and go extraction tips for matrix-assisted laser  
528 desorption/ionization, nanoelectrospray, and LC/MS sample pretreatment in proteomics. *Analytical*  
529 *chemistry* 75: 663-70

530 Ritchie ME, Phipson B, Wu D, Hu Y, Law CW, Shi W, Smyth GK (2015) limma powers differential expression  
531 analyses for RNA-sequencing and microarray studies. *Nucleic acids research* 43: e47

532 Schindler SE, Li Y, Todd KW, Herries EM, Henson RL, Gray JD, Wang G, Graham DL, Shaw LM, Trojanowski  
533 JQ, Hassenstab JJ, Benzinger TLS, Cruchaga C, Jucker M, Levin J, Chhatwal JP, Noble JM, Ringman JM,  
534 Graff-Radford NR, Holtzman DM et al. (2019) Emerging cerebrospinal fluid biomarkers in autosomal  
535 dominant Alzheimer's disease. *Alzheimer's & dementia : the journal of the Alzheimer's Association* 15:  
536 655-665

537 Schirra-Heinen J, Grube L, Waldera-Lupa DM, Baberg F, Langini M, Etemad-Parishanzadeh O, Poschmann  
538 G, Stuhler K (2019) Pitfalls and opportunities in the characterization of unconventionally secreted  
539 proteins by secretome analysis. *Biochimica et biophysica acta Proteins and proteomics* 1867: 140237

540 Schlage P, Kockmann T, Kizhakkedathu JN, auf dem Keller U (2015) Monitoring matrix metalloproteinase  
541 activity at the epidermal-dermal interface by SILAC-iTRAQ-TAILS. *Proteomics* 15: 2491-502

542 Sharma K, Schmitt S, Bergner CG, Tyanova S, Kannaiyan N, Manrique-Hoyos N, Kongi K, Cantuti L, Hanisch  
543 UK, Philips MA, Rossner MJ, Mann M, Simons M (2015) Cell type- and brain region-resolved mouse  
544 brain proteome. *Nature neuroscience* 18: 1819-31

545 Stachel SJ, Coburn CA, Steele TG, Jones KG, Loutzenhiser EF, Gregro AR, Rajapakse HA, Lai MT, Crouthamel  
546 MC, Xu M, Tugusheva K, Lineberger JE, Pietrak BL, Espeseth AS, Shi XP, Chen-Dodson E, Holloway MK,  
547 Munshi S, Simon AJ, Kuo L et al. (2004) Structure-based design of potent and selective cell-permeable  
548 inhibitors of human beta-secretase (BACE-1). *Journal of medicinal chemistry* 47: 6447-50

549 Stiess M, Wegehingel S, Nguyen C, Nickel W, Bradke F, Cambridge SB (2015) A Dual SILAC Proteomic  
550 Labeling Strategy for Quantifying Constitutive and Cell-Cell Induced Protein Secretion. *Journal of*  
551 *proteome research* 14: 3229-3238

552 Stutzer I, Selevsek N, Esterhazy D, Schmidt A, Aebersold R, Stoffel M (2013) Systematic proteomic analysis  
553 identifies beta-site amyloid precursor protein cleaving enzyme 2 and 1 (BACE2 and BACE1) substrates  
554 in pancreatic beta-cells. *The Journal of biological chemistry* 288: 10536-47

555 Suarez-Calvet M, Araque Caballero MA, Kleinberger G, Bateman RJ, Fagan AM, Morris JC, Levin J, Danek A,  
556 Ewers M, Haass C, Dominantly Inherited Alzheimer N (2016) Early changes in CSF sTREM2 in  
557 dominantly inherited Alzheimer's disease occur after amyloid deposition and neuronal injury. *Sci*  
558 *Transl Med* 8: 369ra178

559 UniProt Consortium T (2018) UniProt: the universal protein knowledgebase. *Nucleic acids research* 46:  
560 2699

561 Vassar R, Bennett BD, Babu-Khan S, Kahn S, Mendiaz EA, Denis P, Teplow DB, Ross S, Amarante P, Loeloff  
562 R, Luo Y, Fisher S, Fuller J, Edenson S, Lile J, Jarosinski MA, Biere AL, Curran E, Burgess T, Louis JC et al.  
563 (1999) Beta-secretase cleavage of Alzheimer's amyloid precursor protein by the transmembrane  
564 aspartic protease BACE. *Science (New York, NY* 286: 735-41.

565 Voytyuk I, Mueller SA, Herber J, Snellinx A, Moechars D, van Loo G, Lichtenthaler SF, De Strooper B (2018)  
566 BACE2 distribution in major brain cell types and identification of novel substrates. *Life Sci Alliance* 1:  
567 e201800026-e201800026

568 Wiita AP, Seaman JE, Wells JA (2014) Global analysis of cellular proteolysis by selective enzymatic labeling  
569 of protein N-termini. *Methods in enzymology* 544: 327-58

570 Wolfe CM, Fitz NF, Nam KN, Lefterov I, Koldamova R (2018) The Role of APOE and TREM2 in Alzheimer's  
571 Disease-Current Understanding and Perspectives. *International journal of molecular sciences* 20: 81  
572 Yan R, Bienkowski MJ, Shuck ME, Miao H, Tory MC, Pauley AM, Brashier JR, Stratman NC, Mathews WR,  
573 Buhl AE, Carter DB, Tomasselli AG, Parodi LA, Heinrikson RL, Gurney ME (1999) Membrane-anchored  
574 aspartyl protease with Alzheimer's disease beta-secretase activity. *Nature* 402: 533-7  
575 Yi MH, Zhang E, Kim JJ, Baek H, Shin N, Kim S, Kim SR, Kim HR, Lee SJ, Park JB, Kim Y, Kwon OY, Lee YH, Oh  
576 SH, Kim DW (2016) CD200R/Foxp3-mediated signalling regulates microglial activation. *Scientific  
577 reports* 6: 34901  
578 Yin RH, Yu JT, Tan L (2015) The Role of SORL1 in Alzheimer's Disease. *Molecular neurobiology* 51: 909-18  
579 Zetterberg H, Bendlin BB (2020) Biomarkers for Alzheimer's disease-preparing for a new era of disease-  
580 modifying therapies. *Molecular psychiatry*  
581 Zhang Y, Chen K, Sloan SA, Bennett ML, Scholze AR, O'Keeffe S, Phatnani HP, Guarnieri P, Caneda C,  
582 Ruderisch N, Deng S, Liddelow SA, Zhang C, Daneman R, Maniatis T, Barres BA, Wu JQ (2014) An RNA-  
583 sequencing transcriptome and splicing database of glia, neurons, and vascular cells of the cerebral  
584 cortex. *J Neurosci* 34: 11929-11947  
585 Zielinska DF, Gnad F, Wisniewski JR, Mann M (2010) Precision mapping of an in vivo N-glycoproteome  
586 reveals rigid topological and sequence constraints. *Cell* 141: 897-907

587

588 **Materials and Methods**

589 **Data Availability**

590 The proteomic resource is available for the public on the Proteome Xchange Consortium via the  
591 PRIDE Archive (Project accession: PXD018171).

592 **Mice**

593 All murine samples were isolated from C57BL/6J mice from The Jackson Laboratory according to  
594 the European Communities Council Directive. Mice were housed and breed in the pathogen free  
595 animal facility of the DZNE Munich.

596 **Primary cell culture and brain slices**

597 All primary cultures were maintained under standard cell culture conditions at 37 °C with 5% CO<sub>2</sub>.  
598 The samples were collected from at least two independent culture preparations, with 3 dishes of  
599 primary cells from each culture preparation. It is not possible to determine the sex of the cells,  
600 because the cells were isolated from embryos or young pups. The conditioned media were stored  
601 at -20 °C until further processing.

602 Primary neurons were isolated at E16.5 as described before(Kuhn et al., 2012). Meninges-free  
603 cerebral cortices or hippocampi were dissociated and digested in DMEM with 200 u Papain for 30  
604 min (Sigma Aldrich) and plated into poly-D-lysine coated 6-wells in plaiting media (DMEM + 10%  
605 FBS + 1% penicillin/streptomycin). After 4h media was changed to neuronal cultivation media (B27  
606 + Neurobasal + 0.5 mM glutamine + 1% P/S).

607 Primary astrocytes were isolated at E16.5 and dissociated in the same way as the primary  
608 neurons, however, they were plated on uncoated dishes. Cultures were grown until reaching  
609 confluence in DMEM + 10% FBS, cells were detached using trypsin and re-seeded on a new plate  
610 (50% confluence). This procedure was repeated three times before seeding the cells for the final  
611 experiment (1x10<sup>6</sup> cells into a well of a 6-well plate).

612 Primary oligodendrocyte progenitor cell (OPC) cultures were prepared by magnetic-activated cell  
613 sorting (MACS). 60 mm cell culture dishes were coated with 0.01% poly-L-lysine for 1 h at 37 °C,  
614 washed twice, and incubated with MACS Neuro Medium (Miltenyi Biotec, #130-093-570)  
615 overnight. OPCs were isolated from the brains of postnatal day 6 C57BL/6J mouse pups. Cell  
616 suspension was obtained by automated dissociation using the Neural Tissue Dissociation Kit (P)  
617 (Miltenyi Biotec, Cat#130-092-628) and the gentleMACS™ Dissociator (Miltenyi Biotec, Cat#130-  
618 093-235) following the datasheet of the kit with some modifications. DMEM/pyruvate medium was  
619 used instead of HBSS during tissue dissociation. All media were warmed up to room temperature.  
620 The optional centrifugation steps were included in the dissociation. The myelin removal step was  
621 omitted. Prior to labeling with anti-AN2 MicroBeads (Miltenyi Biotec, Cat#130-097-170), the cell  
622 suspension was incubated with the OPC MACS cultivation medium (MACS Neuro Medium  
623 containing MACS NeuroBrew-21 (Miltenyi Biotec, #130-093-566), GlutaMAX (Thermo Fisher  
624 Scientific, #35050087) and penicillin/streptomycin) for 3h at 37 °C for surface antigen re-  
625 expression. DMEM containing 1% horse serum and penicillin/streptomycin (DMEM/HS medium)  
626 was used as the buffer for magnetic labeling and separation. After magnetic separation, the OPC  
627 MACS cultivation medium was applied to flush out AN2<sup>+</sup> cells. 1x10<sup>6</sup> cells were plated in 4 mL of  
628 OPC MACS cultivation medium per 60mm dish. For OPC/oligodendrocyte culture, ManNAz was  
629 added directly to the medium after one day *in vitro* and incubated for 48h

630 Primary microglia were isolated from postnatal day 5 mouse brains using the MACS technology  
631 as previously described(Daria et al., 2017) Briefly, olfactory bulb, brain stem and cerebellum were  
632 removed and the remaining cerebrum was freed from meninges and dissociated by enzymatic  
633 digestion using the Neural Kit P (Miltenyi Biotec; Cat#130-092-628). Subsequently, tissue was  
634 mechanically dissociated by using three fire-polished glass Pasteur pipettes of decreasing  
635 diameter. Microglia were magnetically labelled using CD11b MicroBeads (Miltenyi Biotec, Cat#  
636 130-093-634) and cell suspension was loaded onto a MACS LS Column (Miltenyi Biotec) and  
637 subjected to magnetic separation. 1.5-2x 10<sup>6</sup> microglia were then cultured in DMEM/F12 media

638 (Invitrogen) supplemented with 10% heat inactivated FBS (Sigma) and 1% Penicillin-Streptomycin  
639 (Invitrogen) in a 60 mm dish for four days before the 48h treatment with ManNAz. Conditioned  
640 media of 1x10<sup>6</sup> cells was used for the hiSPECS experiment.

641 Organotypic brain slice cultures from young (postnatal day 6-7) mice were prepared as described  
642 previously(Daria et al., 2017). Briefly, after brain isolation, olfactory bulb, midbrain, brain stem  
643 and cerebellum were removed and the two remaining cortical hemispheres cut at 350 µm with a  
644 tissue chopper (McIlwain, model TC752, Mickle Laboratory Engineering Company). Intact sagittal  
645 cortico-hippocampal slices were selected and incubated for 30 min at 4°C in a pre-cooled  
646 dissection media (50% HEPES-buffered MEM, 1% penicillin–streptomycin, 10 mM Tris, pH 7.2).  
647 Four slices were then plated onto a 0.4-um porous polytetrafluoroethylene (PTFE) membrane  
648 insert (PICMORG50, Millipore) placed in a 35 mm dish with a slice culture media containing 50%  
649 HEPES-buffered MEM, 25% HBSS, 1 mM L-glutamine (Gibco) and 25% heat-inactivated horse  
650 serum (Merck-Sigma). Media was exchanged one day after preparation and subsequently every  
651 three days. Brain slices were cultured for 14 days before the 48h treatment with ManNAz.

## 652 **hiSPECS**

653 After washing the primary cells with 1x PBS, cell-type specific growth media containing serum  
654 supplements with 50 µM of ManNAz (Thermo Fisher Scientific, Cat#C33366) was added for 48h.  
655 Afterwards, conditioned media was collected and filtered through Spin-X 0.45 µM cellulose acetate  
656 centrifuge tube filter (#8163, Costar) and stored at -20°C in protein Lobind tubes (Eppendorf) until  
657 further usage. Glycoprotein enrichment was performed using 60 µL Concanavalin A (ConA) bead  
658 slurry per sample (Cat#C7555, Sigma Aldrich). ConA beads were washed twice with 1 mL of  
659 binding buffer (5 mM MgCl<sub>2</sub>, 5 mM MnCl<sub>2</sub>, 5 mM CaCl<sub>2</sub>, 0.5 M NaCl, in 20 mM TrisHCL pH 7.5)  
660 before use. The conditioned medium was incubated with the ConA beads for 2h in an overhead  
661 rotator at room temperature. The ConA beads were pelleted by centrifugation (2000 g, 1 min) and  
662 the supernatant containing unbound proteins was discarded. The beads were washed three times

663 with 1 mL binding buffer before adding 500  $\mu$ L of elution buffer (500 mM Methyl-alpha-D-  
664 mannopyranoside, 10 mM EDTA in 20 mM TrisHCl pH 7.5) and rotating over-head for 30 min at  
665 RT. The eluate was filtered through pierce spin columns (Thermo, #69725) to remove remaining  
666 ConA beads and then the filtrate was transferred to a 1.5 mL protein Lobind tube. The elution step  
667 was repeated with another 500  $\mu$ L elution buffer and combined with the first eluate. 50  $\mu$ L of  
668 magnetic DBCO beads (Jena bioscience, Cat#CLK-1037-1) were washed twice with mass spec  
669 grade water and added to the eluate. Sodium deoxycholate (SDC) was added to a final  
670 concentration of 0.1% (w/v) to prevent clumping/sticking of the beads (except otherwise  
671 noted). The click reaction was performed overnight at 4°C on an Eppendorf Thermomixer R shaker  
672 at 1200 rpm to covalently couple metabolically labeled glycoproteins to the magnetic beads. The  
673 next day, beads were washed three times with 1 mL 1% SDS buffer (100mM TrisHCl pH 8.5, 1%  
674 SDS, 250 mM NaCl), three times with 1 mL 8 M UREA buffer (8 M Urea in 100mM TrisHCl pH  
675 8.5) and three times with 1 mL 20% (v/v) acetonitrile. Beads were retained with a magnetic rack  
676 (Dynamag-2, Thermo Scientific). After each step, samples were resuspended briefly by shaking at  
677 1200 rpm at room temperature. Beads were transferred to a new 1.5 mL low binding tube using 2  
678 x 500  $\mu$ L mass spec grade water. Beads were retained in a magnetic rack and the supernatant  
679 was removed. Protein disulfide bonds were reduced in 50  $\mu$ L of 10 mM dithiothreitol (DTT) in  
680 100 mM ammonium bicarbonate (ABC) for 30 min at 1200 rpm at 37°C. Afterwards, the  
681 supernatant was discarded. Alkylation of cysteines was performed using 50  $\mu$ L of 55 mM  
682 iodoacetamide (IAA) in 100mM ABC for 30 min at 1200 rpm and 20°C in the dark. The supernatant  
683 was discarded and beads were washed twice with 100  $\mu$ L of 100 mM ABC. The protein digestion  
684 was performed by adding 0.2  $\mu$ g LysC (Promega) in 50  $\mu$ L of 100 mM ABC for 3h at 1200 rpm at  
685 37°C followed by overnight trypsin digestion using 0.2  $\mu$ g of trypsin (Promega) per sample in 100  
686 mM ABC without 0.1% SDC. The supernatant containing the tryptic peptides was transferred to a  
687 0.5 mL protein Lobind tube. Beads were washed twice with 100 mM ABC without 0.1% SDC and  
688 added to the same tube. Each sample was acidified with 50  $\mu$ L of 8% FA and incubated for 20 min

689 at 4 °C. Precipitated SDC was removed by centrifugation at 18.000 g for 20 min at 4 °C. Peptides  
690 were cleaned up using C18 Stage tips as previously described (Rappaport, Ishihama et al., 2003).  
691 Dried peptides were resuspended in 18 µL 0.1% formic acid (FA) and 2 µL of 1:10 diluted iRT  
692 peptides (Biognosys, Ki-3002-1) were spiked into the samples.

693 **Mass spectrometry**

694 The LC-MS/MS analyses were performed on an EASY-nLC 1200 UHPLC system (Thermo Fisher  
695 Scientific) which was online coupled with a NanoFlex ion source equipped with a column oven  
696 (Sonation) to a Q Exactive™ HF Hybrid Quadrupole-Orbitrap™ mass spectrometer (Thermo Fisher  
697 Scientific). 8 µL per sample were injected. Peptides were separated on a 30 cm self-made C18  
698 column (75 µm ID) packed with ReproSil-Pur 120 C18-AQ resin (1.9 µm, Dr. Maisch GmbH). For  
699 peptide separation, a binary gradient of water and 80% acetonitrile (B) was applied for 120 min at  
700 a flow rate of 250 nL/min and a column temperature of 50 °C: 3% B 0 min; 6% B 2 min; 30% B  
701 92 min; 44% B 112 min; 75% B 121 min.

702 Data dependent acquisition (DDA) was used with a full scan at 120,000 resolution and a scan  
703 range of 300 to 1400 m/z, automatic gain control (AGC) of  $3 \times 10^6$  ions and a maximum injection time  
704 (IT) of 50 ms. The top 15 most intense peptide ions were chosen for collision-induced dissociation  
705 (CID) fragmentation. An isolation window of 1.6 m/z, a maximum IT of 100 ms, AGC of  $1 \times 10^5$  were  
706 applied and scans were performed with a resolution of 15,000. A dynamic exclusion of 120 s was  
707 used.

708 Data independent acquisition (DIA) was performed using a MS1 full scan followed by 20 sequential  
709 DIA windows with variable width for peptide fragment ion spectra with an overlap of 1 m/z covering  
710 a scan range of 300 to 1400 m/z. Full scans were acquired with 120,000 resolution, AGC of  $5 \times 10^6$   
711 and a maximum IT time of 120 ms. Afterwards, 20 DIA windows were scanned with a resolution  
712 of 30,000 and an AGC of  $3 \times 10^6$ . The maximum IT for fragment ion spectra was set to auto to  
713 achieve optimal cycle times. The m/z windows were chosen based on the peptide density map of

714 the DDA run of a representative hiSPECS sample and optimized in a way that allowed the  
715 detection of 8 points per peak. The following window widths were chosen according to the peptide  
716 density map (Fig. 1B):

Window #	1	2	3	4	5	6	7	8	9	10	11	12	13	14	15	16	17	18	19	20
Window Width (m/z)	85	40	30	28	26	25	24	24	24	25	27	28	29	34	38	46	61	151	352	

717

718 The following libraries were used for the different DIA experiments of this manuscript using the  
719 search engine platform MaxQuant and Spectronaut Pulsar X version 12.0.20491.14:

Library	Unique modified peptides	Unique peptide precursors	Protein groups	Used in:
hiSPECS neuron	4,585	5,957	646	Supplementary Table 1+7
hiSPECS brain cell types	12,695	15,886	1,540	Supplementary Table 2
CSF mouse	20,100	24,985	2,550	Supplementary Table 8
hiSPECS slices	2,675	3,375	431	Supplementary Table 9

720

721 **BACE1 inhibitor treatment**

722 The BACE inhibitor C3 ( $\beta$ -secretase inhibitor IV, Calbiochem, Cat#565788, Sigma Aldrich) or  
723 DMSO vehicle control were added in parallel to the ManNAz, at a final concentration of 2  $\mu$ M, to  
724 the neurons for 48h (Kuhn et al., 2012).

725 **LPS treatment of brain slices**

726 Organotypic brain slices were cultured for 2 weeks after the isolation process, followed by a 48 h  
727 ManNAz labelling step. Next, the brain slices were treated for 6 h with LPS (500 ng/mL) followed  
728 by a 24 h collection window of the conditioned media. Serum supplements were not added during  
729 the LPS treatment and the collection period to maximize the inflammatory response. However,  
730 additional ManNAz was added during all steps.

731 **Antibodies**

732 The following antibodies were used for Western Blotting: Mouse monoclonal anti-ADAM22 (UC  
733 Davis/NIH NeuroMab Facility Cat#75-093), Rat monoclonal anti-SEZ6 (Pigoni et al., 2016), Goat

734 polyclonal anti-CD200 (R and D Systems Cat#AF2724,), Rabbit polyclonal anti-calnexin (Enzo  
735 Life Sciences Cat#ADI-SPA-860).

736 **ELISA**

737 CD200 ectodomain levels in the supernatant of primary neurons were measured and quantified  
738 using the following ELISA kit according to the supplier's manual: Mouse CD200 ELISA Kit (LSBio  
739 Cat#LS-F2868). A volume of 250  $\mu$ L from the total of 1 mL undiluted media of 1.5 million primary  
740 cortical neurons cultured for 48h was used per technical replicate. The standard curve provided  
741 with the kit was used and neuronal media which was not cultured with cells, was used as a blank  
742 value.

743 **Western blot analysis**

744 Cells were lysed in STET buffer (50 mM Tris, pH 7.5, 150 mM NaCl, 2 mM EDTA, 1% Triton X-  
745 100), incubated for 20 min on ice with intermediate vortexing. Cell debris as well as undissolved  
746 material was removed by centrifugation at 20,000  $\times$  g for 10 min at 4°C. The protein concentration  
747 was determined using the BC assay kit of Interchim (UP40840A) according to the manufacturer's  
748 instructions. Samples were boiled for 10 min at 95°C in Laemmli buffer and separated on self-cast  
749 8%, 10% or 12% SDS-polyacrylamide gels. Afterwards, proteins were transferred onto  
750 nitrocellulose membranes using a BioRad Wet/Tank Blotting system. The membranes were  
751 blocked for 20 min in 5% milk in 1xPBS with 1% Tween, incubated overnight at 4°C with the  
752 primary antibody, 1h at room temperature with the secondary antibody and developed using an  
753 ECL prime solution (GE Healthcare, RPN2232V1).

754 **Cerebrospinal fluid (CSF) sample preparation**

755 In solution digestion of 5  $\mu$ L CSF samples was performed as previously described (Pigoni et al.,  
756 2016). Dried peptides were dissolved in 18  $\mu$ L 0.1% FA and 2  $\mu$ L 1:10 diluted iRT peptides.

757 **Quantification and statistical analysis**

758 In general, statistical details can be found in the Figure legends including statistical tests and n  
759 number used.

760 **Raw data analysis of mass spectrometry measurements**

761 DDA raw data were analyzed with MaxQuant (version 1.5.5.1 or 1.6.1.0) using the murine UniProt  
762 reference database (canonical, downloaded on: 17.01.2018 which consisted of 16,954 proteins)  
763 and the Biognosys iRT peptide database for label free quantification (LFQ) and indexed retention  
764 time spectral library generation. Default settings were chosen, however, the minimal peptide  
765 length was set to six. Two missed cleavages were allowed, carbamidomethylation was defined as  
766 a fixed modification, and N-termini acetylation as well as oxidation of methionines were set as  
767 variable modifications. The false discovery rate (FDR) was set to less than 1% for protein and  
768 peptide identifications. The results of the MaxQuant analysis were used to generate DIA spectral  
769 libraries of proteins in Spectronaut Pulsar X (Biognosys). Data generated with DIA were analyzed  
770 using Spectronaut Pulsar X (Biognosys) using the self-generated spectral libraries applying  
771 default settings: quantification on the MS2 level of the top N (1 to 3) peptide spectra and a FDR of  
772 1%.

773 **Bioinformatics analysis: Data Pre-processing and Normalization**

774 For the hiSPECS brain secretome resource, the raw dataset was filtered to retain only the proteins  
775 that were consistently quantified in at least 5 of the 6 biological replicates (5/6 or 6/6) in any of the  
776 four cell types. This yielded a total of 995 out of 1083 quantified proteins. The data were further  
777 processed using Perseus (Version 1.6.6.0). The LFQ values were log2 transformed and the  
778 Pearson correlation coefficients between all samples were determined. An imputation procedure  
779 was employed by which missing values are replaced by random values of a left-shifted Gaussian  
780 distribution (shift of 1.8 units of the standard deviation and a width of 0.3).

781 **PCA and UMAP**

782 Principal component analysis and uniform manifold approximation and projection (UMAP) (Diaz-  
783 Papkovich, Anderson-Trocme et al., 2019) were performed to visualize the relationships between  
784 the cell types and between the biological replicates. UMAP is a fast non-linear dimensionality  
785 reduction technique that yields meaningful organization and projection of data points. UMAP has  
786 the advantage of assembling similar individuals (or data points) while preserving long-range  
787 topological connections to individuals with distant relations.

788 **Differential abundance analysis**

789 In order to determine differentially abundant proteins using pairwise comparisons of all four brain  
790 cell types we employed protein-wise linear models combined with empirical Bayes statistics  
791 (implemented in the R package Limma (Ritchie, Phipson et al., 2015), similarly to (Kammers, Cole  
792 et al., 2015)). A protein was considered as differentially abundant (DA) in the different brain cell  
793 types if the Bonferroni-corrected p-value was  $< 0.05$  and the Log2 fold change  $\geq 2$ . The Log2 fold  
794 change of 2 was set to reduce the number of false-positives due to data imputation.

795 **Pathway enrichment score**

796 Proteins were considered to be mainly secreted from one cell type if proteins were identified in at  
797 least 5 out of 6 biological replicates and fulfilled one of following criteria: 1) proteins were only  
798 detected in two or less biological replicates in another cell type or 2) proteins were at least 5-fold  
799 enriched in a pairwise comparison to all three other cell types.

800 Functional annotation clustering of proteins specifically secreted from each cell type was  
801 performed with DAVID 6.8 (Huang da, Sherman et al., 2009a, Huang da, Sherman et al., 2009b)  
802 using all 995 robustly quantified proteins in the hiSPECS secretome resource as the background.  
803 The top three gene ontology terms for biological process (GOTERM\_BP\_FAT) were picked for  
804 visualization based on the enrichment score using medium classification stringency. The same  
805 settings were chosen to identify functional annotation clusters of all proteins in the hiSPECS library

806 identified compared to the whole mouse proteome for the gene ontology term cellular  
807 compartment (GOTERM\_CC\_FAT).

808 **Comparison of secretome proteins to their relative abundances in the corresponding cell  
809 lysates using a published database**

810 We compared our cell type-specific secretome proteins to the corresponding cell type-specifically  
811 expressed proteins identified in cell lysates of the same four cultured primary brain cell types in a  
812 previous proteomic study(Sharma et al., 2015). The data from their study containing the LFQ  
813 values of the individual biological replicates of the brain cell lysate were downloaded (Sharma et  
814 al.: Supplementary Table 1) and processed using Perseus. Proteins detected in at least one cell  
815 type with two biological replicates were considered and missing values were imputed as described  
816 before (replacement of missing values from left-shifted normal distribution, 1.8 units of the  
817 standard deviation and a width of 0.3). Proteins with 2.5-fold higher protein levels in one cell type  
818 as compared to all other three cell types were considered specific. On the basis of this analysis,  
819 we defined two categories: 1) proteins that were specifically enriched in one cell type both in cell  
820 lysates and the corresponding cell secretome and 2) cell type-specifically secreted proteins that  
821 were not enriched in the corresponding lysate. The second category indicates a possible  
822 secretome-specific mechanism, such as the selective secretion/shedding by a protease in the  
823 given cell type.

824 **Interactions with cell lysate proteins detected by Sharma et. al**

825 To find the relationships between the proteins in the secretome and those from the cell lysate,  
826 we searched for interacting partners of the proteins specifically enriched in the secretome of a  
827 specific cell type and the proteins from the cell lysate as determined by (Sharma et al., 2015).  
828 We downloaded the mouse protein-protein interaction network (PPIN) from BioGRID (Chatr-  
829 Aryamontri et al., 2015) and additional binary interactions data from UniProt (UniProt  
830 Consortium, 2018).

831 **Disease association**

832 To determine if the proteins significantly differentiated in one cell type with respect to the other 3  
833 cell types are linked to neurodegenerative diseases, we searched for curated gene disease  
834 associations (GDA) from DisGeNET (Pinero et al., 2017). Our search list contained 31 known  
835 diseases of the nervous system. We set the evidence index (EI) to 0.95: an EI of 1 indicates that  
836 all the available scientific literature supports the specific GDA.

837

838 **Supplementary Information titles and legends**

839 **Overview Supplementary Tables:**

840 Supplementary Table 1: Comparison of the SPECS and hiSPECS method using DIA and DDA.

841 Related to Fig. 1.

842 Supplementary Table 2: hiSPECS secretome resources of astrocytes, microglia, neurons and

843 oligodendrocytes. Related to Fig. 2.

844 Supplementary Table 3: Meta-analysis of brain cell lysate data and its comparison to the

845 secretome resource. Related to Fig. 2,4.

846 Supplementary Table 4: Cell type-specifically secreted proteins of the hiSPECS secretome

847 resource.

848 Related to Fig. 2-7.

849 Supplementary Table 5: Interaction analysis of cell type-specific secretome and transmembrane

850 lysate proteins. Related to Fig. 3.

851 Supplementary Table 6: hiSPECS analysis of BACE1 inhibitor treated neurons vs. control.

852 Related to Fig. 5.

853 Supplementary Table 7: List of BACE1 substrate candidates.

854 Related to Fig. 5.

855 Supplementary Table 8: Murine CSF analysis and comparison to the cell type-resolved

856 secretome resource. Related to Fig. 6.

857 Supplementary Table 9: hiSPECS analysis of brain slices.

858 Related to Fig. 7

859 **Figure legends**

860 **Fig. 1: Workflow of the hiSPECS method and benchmarking against SPECS.**

861 **A)** Graphical illustration of the hiSPECS workflow. Cells are metabolically labeled with N-azido-  
862 mannosamine (ManNAz), an azido group-bearing sugar, which is metabolized in cells and  
863 incorporated as azido-sialic acid into N- and O-linked glycans of newly synthesized glycoproteins,  
864 but not into exogenously added serum proteins.

865 **B)** Bar chart indicating protein quantification, protein localization (according to UniProt) in the  
866 secretome of primary neurons, comparing the previous SPECS (blue) to the new hiSPECS  
867 method using DDA (light green) or DIA (dark green). Proteins were counted if quantified in at least  
868 9 of the 11 biological replicates of hiSPECS or 4 of 5 biological replicates of the previous SPECS  
869 paper (Kuhn et al., 2012). The category glycoprotein\* includes UniProt annotations and proteins  
870 annotated as glycoproteins in previous papers(Fang et al., 2016, Joshi et al., 2018, Liu et al.,  
871 2017, Zielinska et al., 2010). Proteins can have multiple UniProt annotations, e.g. for APP  
872 membrane, TM, cytoplasm and nucleus, because distinct proteolytic fragments are found in  
873 different organelles, so that some proteins in categories cytoplasm and nucleus may overlap with  
874 the categories secreted and TM+GPI.

875 **C)** Venn diagram comparing the number of protein groups quantified (5/6 biological replicates) by  
876 DDA versus DIA of the same samples. Left panel: glycoprotein. Right panel: TM and GPI proteins,  
877 which are potentially shed proteins.

878 **D)** Distribution of quantified proteins with DDA and DIA (at least in 3 of 6 biological replicates).  
879 The number of quantified proteins is plotted against the log10 transformed label-free quantification  
880 (LFQ) values with a bin size of 0.5. The number of quantified proteins per bin for DDA and DIA  
881 are indicated in light and dark green, respectively. Proteins that were only quantified with DDA or  
882 DIA are colored in light and dark purple, respectively. DIA provides additional quantifications for

883 low abundant proteins and extends the dynamic range for protein quantification by almost one  
884 order of magnitude.

885 **E)** All tryptic peptides identified from TM proteins were mapped onto their protein domains. Only  
886 0.1% of the peptides mapped to intracellular domains. Demonstrating that secretome proteins  
887 annotated as TM proteins comprise the shed ectodomains, but not the full-length forms of the  
888 proteins.

889 **F)** Comparison of SPECS and hiSPECS method with regard to cell number, volume of culture  
890 media, sample preparation time and mass spectrometer measurement time.

891 TM: single-pass transmembrane protein; GPI: Glycosylphosphatidylinositol-anchored membrane  
892 protein.

893 **Fig. 2: Cell type-resolved mouse brain secretome resource**

894 **A)** Illustration of the proteomic resource including secretome analysis of primary murine  
895 astrocytes, microglia, neurons, oligodendrocytes, cerebrospinal fluid (CSF) analysis and brain  
896 slices (hippocampus (Hip), cortex (Ctx)).

897 **B)** Number of peptides (left) and protein groups (right) quantified in the secretome of the  
898 investigated brain cell types with the hiSPECS DIA method. Proteins quantified in at least 5 out of  
899 6 biological replicates in at least one cell type are considered. In total 995 protein groups were  
900 detected.

901 **C)** 995 proteins were quantified and identified (ID) in the hiSPECS secretome resource. The grey  
902 part of each column indicates how many proteins were also detected in the lysates of the same  
903 four cell types as analyzed in a previous proteome dataset(Sharma et al., 2015). This reveals that  
904 111 proteins (purple) were only detected in the secretome. Relative to all the secretome proteins  
905 covered by the lysate study (grey) the most enriched UniProt annotation of the newly identified  
906 proteins (purple) was secreted and extracellular matrix (15%) (lower panel).

907 **D)** Correlation matrix showing the relationship between the different brain cell types. The matrix  
908 shows the Pearson correlation coefficient (red indicates a higher, blue a lower correlation) and the  
909 correlation plots of the log2 LFQ intensities of the secretome of astrocytes, neurons, microglia and  
910 oligodendrocytes processed with the hiSPECS method.

911 **E)** UMAP (Uniform Manifold Approximation and Projection) plot showing the segregation of the  
912 brain cell type secretomes based on LFQ intensities of quantified proteins.

913 **F)** Venn diagram illustrating the percentage of the secretome proteins which were secreted from  
914 only one or multiple cell types. Proteins quantified in at least 5 biological replicates of one cell type  
915 were considered.

916 **G)** Bar graph indicating the number of protein groups, which were detected in one, two, three or  
917 all cell types with at least 5 biological replicates.

918 **Fig. 3: Cell type-specific enrichment of proteins in the secretome of brain cells.**

919 **A)** Heat map of the hiSPECS library proteins across the four cell types from hierarchical clustering.  
920 For missing protein data, imputation was performed. Rows represent the 995 proteins and  
921 columns represent the cell types with their replicates. The colors follow the z-scores (blue low,  
922 white intermediate, red high). Functional annotation clustering with DAVID 6.8(Huang da et al.,  
923 2009a, Huang da et al., 2009b) for the gene ontology category biological process (FAT) of protein  
924 clusters enriched in one cell type are indicated on the right sorted by the enrichment score  
925 (background: all proteins detected in the hiSPECS brain secretome resource).

926 **B)** Interaction map of the hiSPECS secretome and the published lysate proteome data(Sharma et  
927 al., 2015) illustrating the cellular communication network between the major brain cell types.  
928 Interaction pairs are based on binary interaction data downloaded from UniProt and BioGRID  
929 databases (Chatr-Aryamontri et al., 2015, UniProt Consortium, 2018). Cell type-specifically  
930 secreted proteins of the hiSPECS secretome resource were mapped to their interaction partners

931 if the interaction partners also show cell type-specificity in lysates of one brain cell type in the  
932 proteome data(Sharma et al., 2015) (2.5-fold pairwise) and are annotated as transmembrane  
933 protein in UniProt (Supplementary Table 5).

934 **C)** Visualization of the glycoproteins detected in at least 5 of 6 biological replicates of the four  
935 brain cell types. Soluble secreted or potentially shed proteins are indicated for each cell type. The  
936 radius of the circles resembles the protein count. Shed proteins: includes proteins annotated as  
937 single-pass transmembrane and glycosylphosphatidylinositol (GPI)-anchored proteins, of which  
938 the shed ectodomain was found in the secretome; Sec: soluble secreted.

939 **D)** Visualization of the cell type specific (CTS) glycoproteins as in C), either specifically secreted  
940 by one cell type in at least 5 biological replicates and no more than 2 biological replicates in  
941 another cell type or 5-fold enriched according to pairwise comparisons to the other cell types  
942 (Supplementary Table 4).

943 **Fig. 4: Protein levels in the brain cell secretome vs. lysate proteome.**

944

945 **A)** Bar graph of proteins specifically secreted from the indicated cell types. The solid part of the  
946 box indicates which fraction of proteins were predominantly enriched both in the secretome and  
947 the lysate of the indicated cell type, suggesting that cell type-specific secretion results from cell  
948 type-specific protein synthesis. The light part of the box shows the fraction of proteins that were  
949 specifically secreted from the indicated cell type, although this protein had similar levels in the  
950 lysate of multiple cell types, indicating cell type-specific mechanisms of secretion or shedding.

951 Lysate protein levels were extracted from (Sharma et al., 2015).

952 **B-C)** Comparison of the hiSPECS secretome resource and lysate data by (Sharma et al., 2015).  
953 The % enrichment is indicated normalized to the average of the most abundant cell type. B)  
954 TREM2 and CD200 are jointly enriched in both secretome and lysate in microglia or neurons,  
955 respectively. In C) two examples, of proteins specifically enriched in the secretome, but not in the

956 lysate are shown. ADIPOQ is specifically secreted from oligodendrocytes, but reveals highest  
957 expression in astrocytes. CACHD1 is specifically secreted from neurons, but high protein levels  
958 can be found in astrocytes, neurons and oligodendrocytes.

959 **Fig. 5: Identification and validation of substrate candidates of the protease BACE1.**

960 **A)** Experimental design of the ManNAz labeling step and BACE1 inhibitor C3 treatment of the  
961 primary neuronal culture for 48h at 5 to 7 days in vitro (DIV).

962 **B)** Volcano plot showing changes in protein levels in the secretome of primary neurons upon  
963 BACE1 inhibitor C3 treatment using the hiSPECS DIA method. The negative log10 p-values of all  
964 proteins are plotted against their log2 fold changes (C3 vs control). The grey hyperbolic curves  
965 depict a permutation based false discovery rate estimation ( $p = 0.05$ ;  $s_0 = 0.1$ ). Significantly  
966 regulated proteins ( $p < 0.05$ ) are indicated with a dark blue dot and known BACE1 substrates are  
967 indicated with blue letters. The two newly validated BACE1 substrates CD200 and ADAM22 are  
968 indicated in red.

969 **C)** Independent validation of the novel BACE1 substrate candidates CD200 and ADAM22 by  
970 Western blotting in supernatants and lysates of primary neurons incubated with or without the  
971 BACE1 (B1) inhibitor C3 for 48h. Full-length (fl) ADAM22 and CD200 levels in the neuronal lysate  
972 and were mildly increased upon BACE1 inhibition, as expected due to reduced cleavage by  
973 BACE1. Calnexin served as a loading control. The soluble ectodomain of ADAM22 (sADAM22)  
974 was strongly reduced in the conditioned medium upon BACE1 inhibition. Ectodomain levels of the  
975 known BACE1 substrate SEZ6 (sSEZ6) were strongly reduced upon BACE1 inhibition and served  
976 as positive control.

977 **D)** Quantification of the Western blots in C). Signals were normalized to calnexin levels and  
978 quantified relative to the control (ctr) condition. Statistical testing was performed with  $N=6$   
979 biological replicates, using the one sample t-test with the significance criteria of  $p < 0.05$ .  
980 According to this criterion, ADAM22 and CD200 were significantly increased in total lysates upon

981 C3 treatment (fADAM22: p-value 0.0251, fCD200: p-value 0.011). Soluble ADAM22 was  
982 significantly reduced in the supernatant upon C3 treatment (p-value <0.0001).

983 **E)** The reduction of the soluble ectodomain of CD200 (sCD200) was detected by ELISA, because  
984 the available antibodies were not sensitive enough for Western blots of the conditioned medium.

985 **F)** Extracted ion chromatogram of the semi-tryptic peptide of CD200 in conditioned media of  
986 neurons comparing C3-treated to control condition. Levels of the semi-tryptic peptide were  
987 strongly reduced upon BACE1 inhibition.

988 **G)** The potential cleavage site of CD200 was identified by a semi-tryptic peptide indicated in red  
989 which is from the juxtamembrane domain of CD200. The transmembrane domain is indicated in  
990 blue. The semi-tryptic peptide was found i) using the hiSPECS method in the neuronal secretome  
991 under control conditions but not upon BACE1 inhibition, and ii) in the CSF of wildtype mice but not  
992 upon knockout of BACE1 and its homolog BACE2 – \*data are extracted from (Pigoni et al., 2016).  
993 Because BACE2 is hardly expressed in brain, both data sets demonstrate that generation of the  
994 semi-tryptic peptide requires BACE1 activity and thus, represents the likely BACE1 cleavage site  
995 in CD200.

996 **Fig. 6: Mapping of murine CSF proteins to their probable cell type origin.**

997 **A)** Protein dynamic range plot of the log10 transformed LFQ intensities of the murine CSF proteins  
998 quantified in at least 3 of 4 biological replicates measured with DIA. The proteins are split into  
999 quartiles according to their intensities, with the 1st quartile representing the 25% most abundant  
1000 proteins. The percentage of proteins annotated in UniProt with the following subcellular  
1001 locations/keywords are visualized for: membrane, secreted, cytoplasm, and glycoprotein.

1002 **B)** Protein dynamic range plot of the log10 transformed LFQ intensities specifically of  
1003 glycoproteins in the murine CSF quantified in at least 3 of 4 biological replicates measured with  
1004 DIA. The proteins are split into quartiles according to their intensities. The percentage of proteins

1005 identified in the secretome of astrocytes, microglia, neurons or oligodendrocytes in at least 5 of 6  
1006 biological replicates is illustrated below. Selected proteins specifically secreted from one cell type  
1007 are indicated with the color code of the corresponding cell type.

1008 **C)** Venn diagram indicating the distribution of CSF glycoproteins detected in the hiSPECS  
1009 secretome resource.

1010 **D)** Cell type specifically secreted proteins (CTSP) in the hiSPECS secretome study (5-fold  
1011 enriched in pairwise comparison to the other cell types or only detected in one cell type) are listed  
1012 according to their presence in the CSF quartiles.

1013 **E)** List of proteins detected in murine CSF and the hiSPECS secretome resource which have  
1014 human homologs that are linked to brain disease based on the DisGeNet database(Pinero et al.,  
1015 2017) with an experimental index, e.i  $\geq 0.9$ . Relative protein levels in the brain cell secretome is  
1016 indicated (black high, white low abundance). Colored gene names indicate cell type-specific  
1017 secretion.

1018 **Fig. 7: The secretome of brain slices.**

1019 **A)** hiSPECS DDA and DIA analysis of brain slice cultures in the presence of 25% serum. The bar  
1020 chart comparing the hiSPECS DDA and DIA method indicates the protein number and their  
1021 localization according to UniProt identified in the secretome of brain slices. Proteins quantified in  
1022 at least 5 of 6 biological replicates are considered.

1023 **B)** Protein dynamic range plot of the log10 LFQ intensities of secretome proteins of brain slices in  
1024 descending order. According to their intensity, proteins are grouped into quartiles and the  
1025 percentage of proteins with the following UniProt keywords is visualized: membrane, secreted,  
1026 cytoplasm. The percentage of proteins identified in the secretome of astrocytes, microglia,  
1027 neurons or oligodendrocytes in at least 5 of 6 biological replicates is illustrated. Selected proteins

1028 specifically secreted from one cell type are indicated with the color code of the corresponding cell  
1029 type.

1030 **C)** Cell type-specifically secreted proteins according to the hiSPECS secretome resource (5-fold  
1031 enriched in pairwise comparison to the other cell types or consistently detected only in one cell  
1032 type; Supplementary Table 4) detected in the secretome of brain slices.

1033 **D)** Volcano plot showing changes in protein levels in the secretome of primary cultured brain slices  
1034 upon 6 h LPS treatment in a 24 h collection window using the hiSPECS DIA method. The negative  
1035 log10 p-values of all proteins are plotted against their log2 fold changes (LPS vs control). The grey  
1036 hyperbolic curves depict a permutation based false discovery rate estimation ( $p = 0.05$ ;  $s_0 = 0.1$ ).  
1037 Significantly regulated proteins ( $p < 0.05$ ) are indicated with a dark blue dot. Proteins highlighted in  
1038 red indicate proteins known to increase upon LPS treatment (Meissner et al., 2013) for details see  
1039 Supplementary Table 9.

1040 **E-F)** Significantly regulated proteins upon LPS treatment ( $p < 0.05$ ) of brain slices split according  
1041 to UniProt keywords membrane, single-pass transmembrane and GPI-anchored, and secreted  
1042 proteins; F) indicating cell type specificity in the hiSPECS secretome resource.

1043

1044 **Supplemental Figure legends**

1045 **Supplementary Fig. 1: Benchmarking hiSPECS against SPECS.**

1046 **A)** Comparison of the novel iSPECS (green) and the previous SPECS (blue) protocol (Kuhn et al.,  
1047 2012). hiSPECS uses lectin-based glycoprotein enrichment followed by covalent binding to  
1048 magnetic beads which improves sample processing. On-bead tryptic digestion is followed by mass  
1049 spectrometry analysis and label-free quantification (LFQ) using data independent or data  
1050 dependent acquisition (DIA vs DDA). In contrast, SPECS depends on biotinylation of the azide-  
1051 functionalized glycoproteins, followed by streptavidin pull down, SDS-gel based fractionation into  
1052 14 gel slices and DDA analysis only.

1053 **B)** Coomassie stained gel showing the prominent reduction of albumin as a result of glycoprotein  
1054 enrichment with ConA. Left lane: secretome (conditioned medium) of primary neurons before  
1055 glycoprotein enrichment. 10% of the volume was loaded that was used for the ConA enrichment.  
1056 Right lane: eluate after glycoprotein enrichment using ConA beads. The albumin band is  
1057 highlighted with a red arrow.

1058 **C)** A representative peptide density plot of a neuronal secretome using the hiSPECS method and  
1059 analyzed in DDA mode. The m/z ratio is plotted against the retention time. One MS1 scan (purple)  
1060 is followed by 20 MS2 scans covering a range of 300 to 1400 m/z with an overlap of 1 m/z between  
1061 adjoining m/z windows. The m/z windows were adjusted to achieve equal numbers of peptides.

1062 **D)** Identified glycoproteins in the secretome of primary neurons using the DIA hiSPECS protocol  
1063 according to UniProt or (Fang et al., 2016, Joshi et al., 2018, Liu et al., 2017, Zielinska et al.,  
1064 2010).

1065 **E)** Venn diagram illustrating in which sources the proteins of D) were found to contain a  
1066 glycosylation site. As expected for the glyco-secretome, more than 85% of the quantified  
1067 secretome proteins were annotated as glycoproteins.

1068 **F)** Representative Pearson correlations of log2 transformed protein LFQ intensities of four  
1069 biological replicates (BR) either processed with the SPECS or hiSPECS method. In the previous  
1070 SPECS studies sample pairs were separated on the same gel to achieve high reproducibility,  
1071 whereas the correlation of biological replicates run on different gels was rather low. Thus, protein  
1072 LFQ ratios of the individual replicates were used for statistical evaluation. The blue squares  
1073 indicate samples run on the same gel during sample preparation (SPECS data obtained from  
1074 (Kuhn et al., 2012)).

1075 **Supplementary Fig. 2: Quality control of cell type-resolved mouse brain secretome  
1076 resource.**

1077 **A)** Data transformation of the hiSPECS DIA secretome analysis of the brain cell types. Log2  
1078 Transformation of the label free quantification values (LFQ).

1079 **B)** Functional annotation clustering with DAVID 6.8 (Huang da et al., 2009a, Huang da et al.,  
1080 2009b) for gene ontology term cellular component (FAT) of the 995 hiSPECS proteins identified  
1081 using the mouse proteome as background. The dot sizes indicate the log 2 enrichment score.

1082 **C)** Fold change of cell type specific proteins in the brain cells. Log2 ratio of the average abundance  
1083 in the specific cell type to the median abundance in the other cell types in the hiSPECS secretome  
1084 or lysate analysis (Sharma et al., 2015) is shown. Known cell type-specific marker proteins are  
1085 highlighted for each cell type which reveal a strong enrichment in the lysate and secretome of the  
1086 primary brain cells verifying the quality and comparability of the primary cultures. For example, the  
1087 ectodomain of the membrane protein NCAM2 (with an y-axis value of 3 in the log2 scale) is  
1088 secreted about 8-fold more from oligodendrocytes compared to the median of the other three cell  
1089 types.

1090 **D) Principal component analysis (PCA).** The secretomes of the four cell types segregated based  
1091 on the two major components of all 995 proteins identified in at least 5 biological replicates in one  
1092 cell type, which accounted for 44.9% and 19% of the variability, respectively.

1093 **Supplementary Fig. 3: Diversity of cell type-resolved mouse brain glyco-secretome  
1094 resource.**

1095 Pairwise comparison of the secretomes of the four different cell types. Volcano plot indicating the  
1096 proteins in the conditioned media of the different primary brain cells analyzed with the hiSPECS  
1097 DIA method. The negative log10 transformed p-value of each protein is plotted against its log2  
1098 fold change comparing all investigated cell types with each other. Significantly regulated proteins  
1099 ( $p\text{-value} < 0.05$ ) are indicated in dark blue. The grey hyperbolic curves depict a permutation based  
1100 false discovery rate estimation ( $p = 0.05$ ;  $s_0 = 0.1$ ).

1101 **Supplementary Fig. 4: Top 50 cell type-specifically enriched proteins in the secretome  
1102 resource.**

1103 **A)** Heat map of the top 50 differentially secreted proteins (Bonferroni  $p\text{-adj} < 0.05$ ) across the four  
1104 cell types from hierarchical clustering. For the missing protein quantification data, an imputation  
1105 approach was undertaken using data missing at random within a left-shifted Gaussian distribution  
1106 by 1.8 standard deviation. The rows represent the differentially secreted proteins and the columns  
1107 represent the cell types with their replicates. The colors represent log-scaled protein levels with  
1108 blue indicating the lowest, white indicating intermediate, and red indicating the highest protein  
1109 levels.

1110 **B)** Functional annotation clustering with DAVID 6.8 (Huang da et al., 2009a, Huang da et al.,  
1111 2009b) for gene ontology term biological process (FAT) of the cell type-specific secretome proteins  
1112 (Supplementary Table 4). All proteins detected in the hiSPECS brain secretome study have been  
1113 chosen as the background. The dot sizes indicate the enrichment score.

1114 **Supplementary Fig. 5: Protein levels in the brain cell secretome vs lysate proteome.**

1115 Comparison of the iSPECS secretome resource and lysate data by (Sharma et al., 2015). The %  
1116 enrichment is indicated normalized to the average of the most abundant cell type. For example,  
1117 APLP1 is similarly abundant in lysates of neurons and oligodendrocytes, but only secreted to a  
1118 relevant extent from neurons. Thus, APLP1 is classified as a cell type-specifically secreted protein.

1119 **Supplementary Fig. 6: Substrate candidate identification of the Alzheimer's protease**  
1120 **BACE1 as proof of principle of the iSPECS method.**

1121 **A)** Same experiment as in Fig. 2A,B, but using DDA instead of DIA for mass spectrometric data  
1122 acquisition. The volcano plot shows changes in protein levels in the secretome of primary cultured  
1123 neurons upon BACE1 inhibitor C3 treatment using the iSPECS DDA method. The negative log10  
1124 transformed p-value of each protein is plotted against its log2 fold change comparing inhibitor  
1125 treated and control condition. The grey hyperbolic curves depict a permutation based false  
1126 discovery rate estimation ( $p = 0.05$ ;  $s_0 = 0.1$ ). Significantly regulated proteins ( $p < 0.05$ ) are  
1127 indicated with a dark blue dot and known BACE1 substrates are indicated with blue letters. The  
1128 two newly validated BACE1 substrates CD200 and ADAM22 are indicated in red. SEZ6 and IL6ST  
1129 are not depicted in the volcano plot because they were only identified in the control condition.

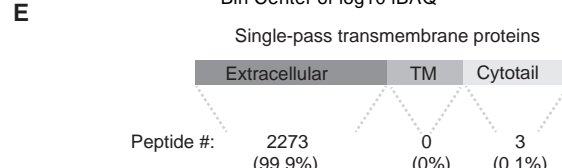
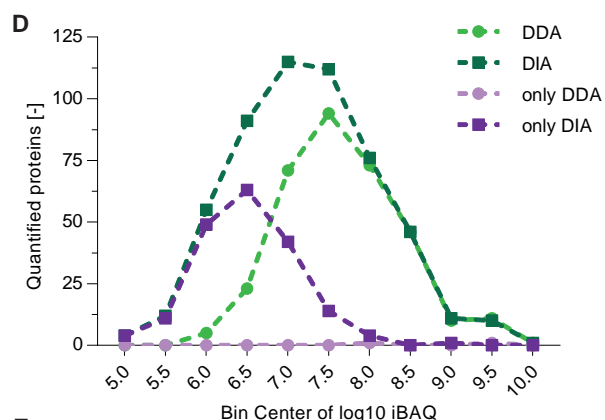
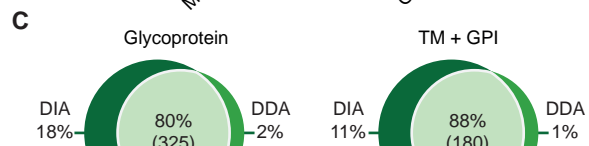
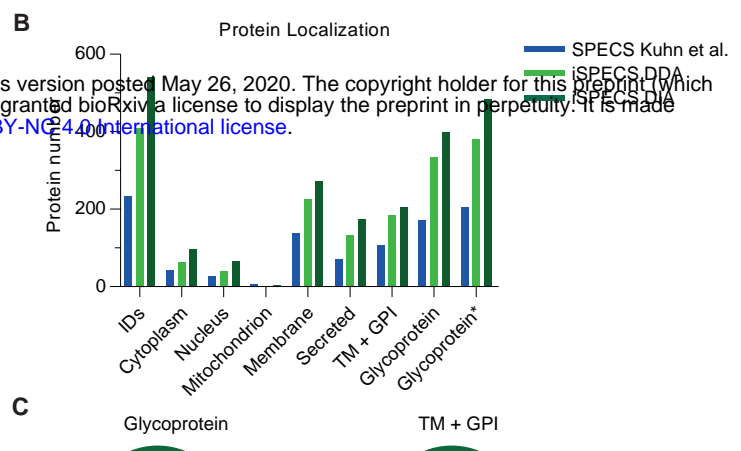
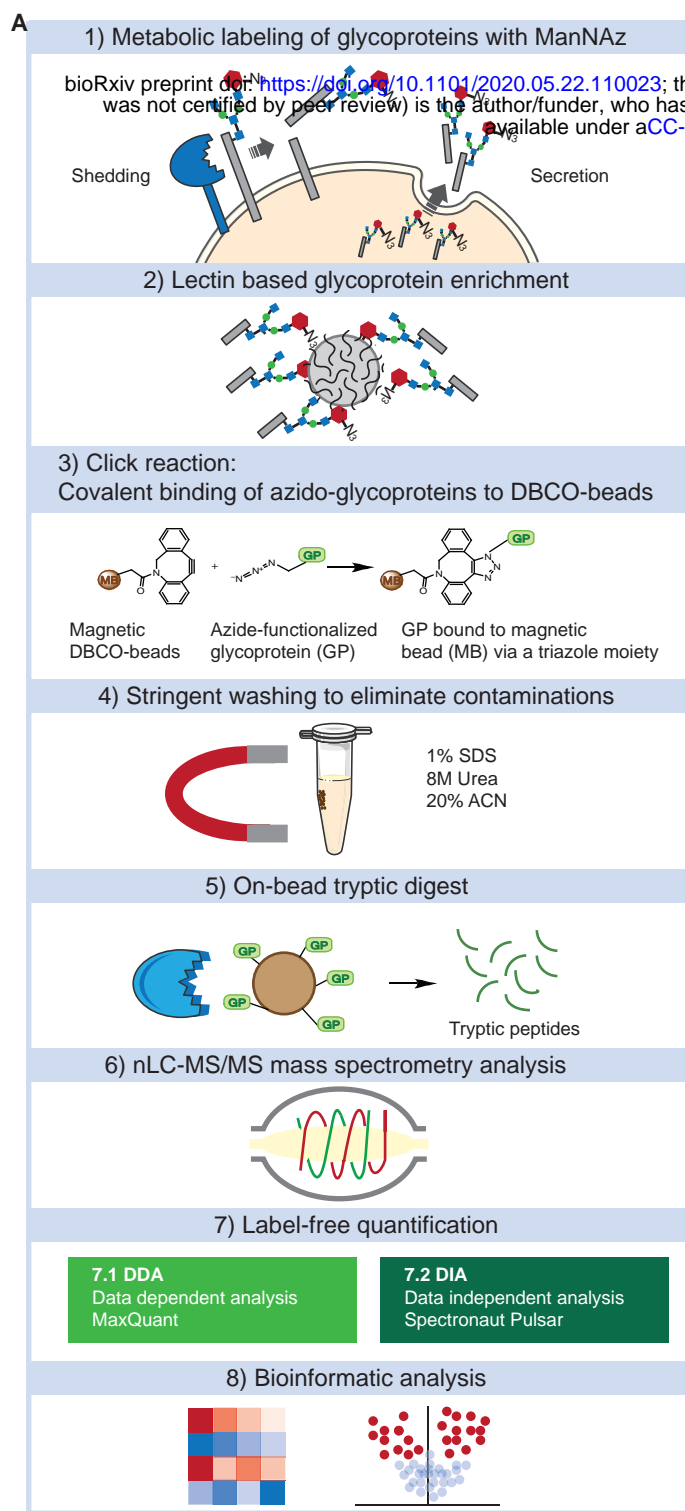
1130 **B)** Correlation of the hiSPECS DDA to DIA method. Plotted are the log2 fold changes between  
1131 C3 treatment and DMSO control samples (N=11).

1132 **Supplementary Fig. 7: Top25 enriched proteins in the secretome of astrocytes, microglia,**  
1133 **neurons and oligodendrocytes.**

1134 Representation of the top 25 glycoproteins enriched in the secretome of one cell type. The average  
1135 log2 LFQ intensities are plotted against the log2 LFQ ratios of the cell type specific-abundance  
1136 subtracted from the average of the other cell types. Therefore, the values on the y-axis roughly  
1137 indicate the abundance within a cell's secretome, whereas the values on the x-axis show the

1138 enrichment compared to the other cell types in log2 scale. Yellow circles indicate proteins which  
1139 are also detected in murine CSF. One example is HEXB in the microglia panel with an average  
1140 LFQ value of 21.2 (y-axis) and a value of 5.4 on the x-axis. This indicates that the protein has a  
1141  $2^{5.4}$ -fold higher level in the secretome of microglia compared to the average of its levels in the  
1142 secretome of the other three cell types.

**Figure 1: Workflow of the hiSPECS method and benchmarking against SPECS.**



**F**

	SPECS	iSPECS	fold reduction
Cell number per sample	$40 \times 10^6$	$1 \times 10^6$	40
Volume cell media per sample	40 mL	1 mL	40
Sample preparation time for 12 samples	15 d	3 d	5
Measurement time for 12 samples	7.5 d	1.5 d	5

**Figure 2: Cell type-resolved mouse brain glyco-secretome resource**

bioRxiv preprint doi: <https://doi.org/10.1101/2020.05.22.110023>; this version posted May 26, 2020. The copyright holder for this preprint (which was not certified by peer review) is the author/funder, who has granted bioRxiv a license to display the preprint in perpetuity. It is made available under aCC-BY-NC 4.0 International license.

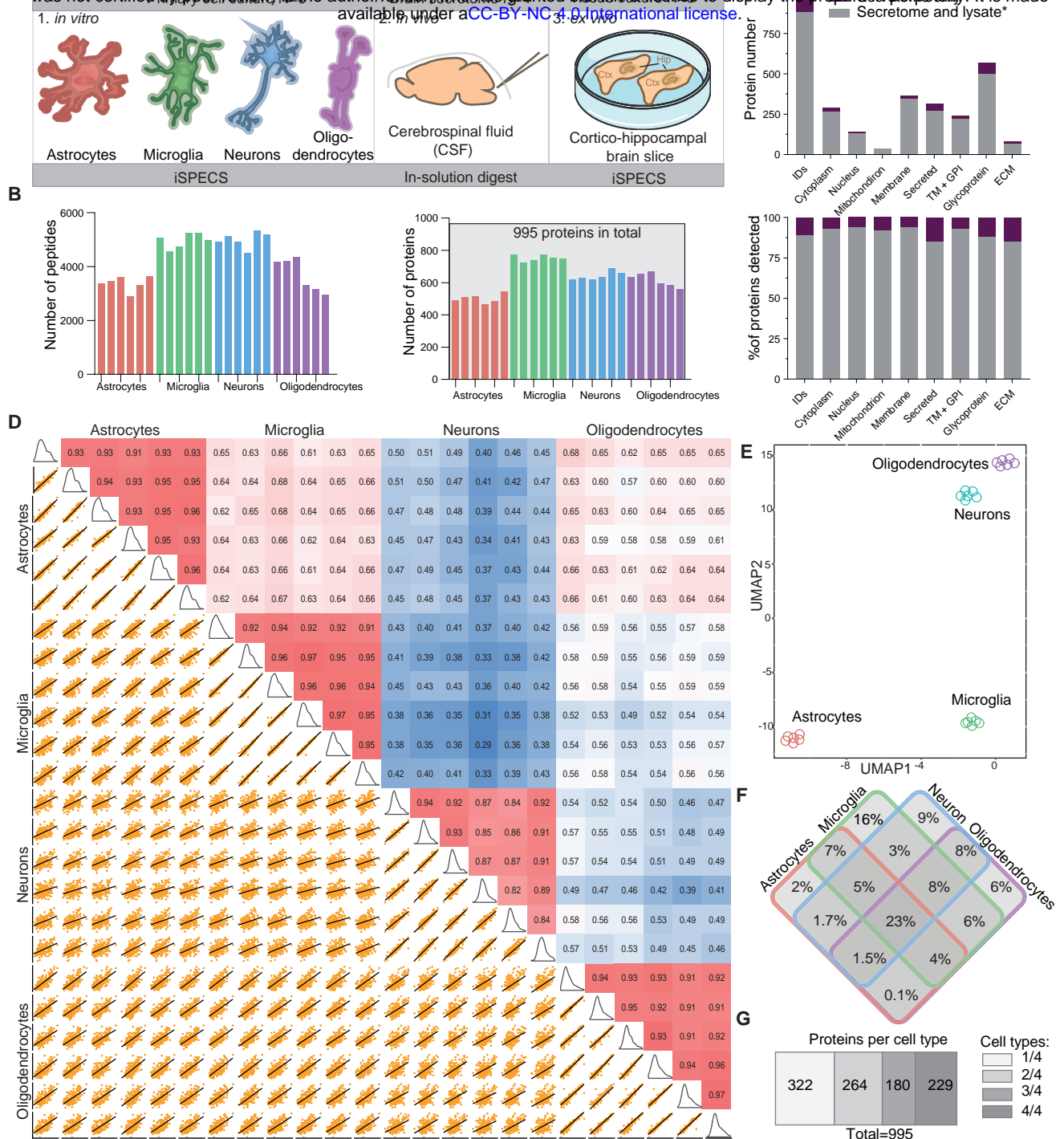
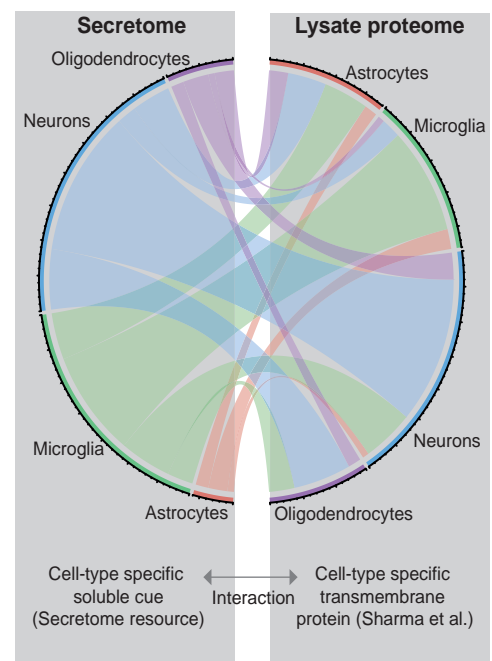
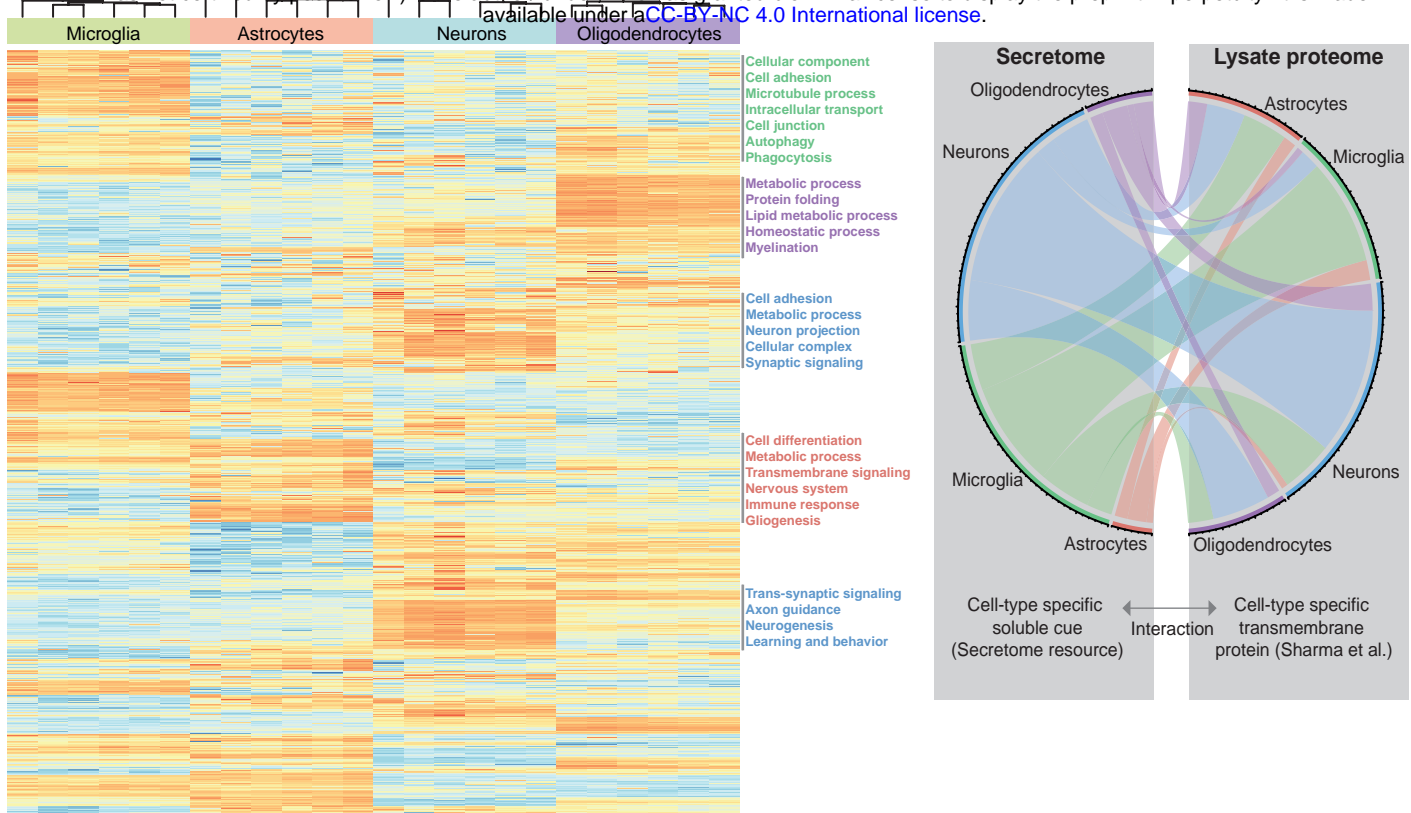
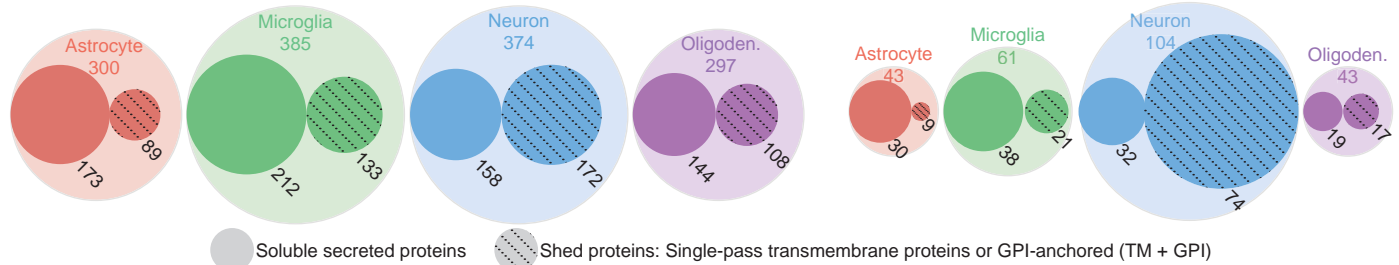


**Figure 3: Cell type-specific enrichment of proteins in the secretome of brain cells.**

**A** bioRxiv preprint doi: <https://doi.org/10.1101/2020.05.22.110023>; this version posted May 26, 2020. The copyright holder for this preprint (which was not certified by peer review) is the author/funder, who has granted bioRxiv a license to display the preprint in perpetuity. It is made available under aCC-BY-NC 4.0 International license.



**C** Glycoproteins detected in one cell type



**D** Cell type-specifically secreted glycoproteins

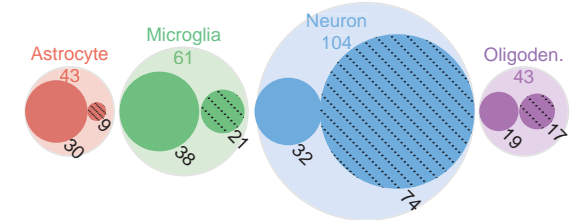


**Figure 4: Protein levels in the brain cell secretome vs. lysate proteome.**

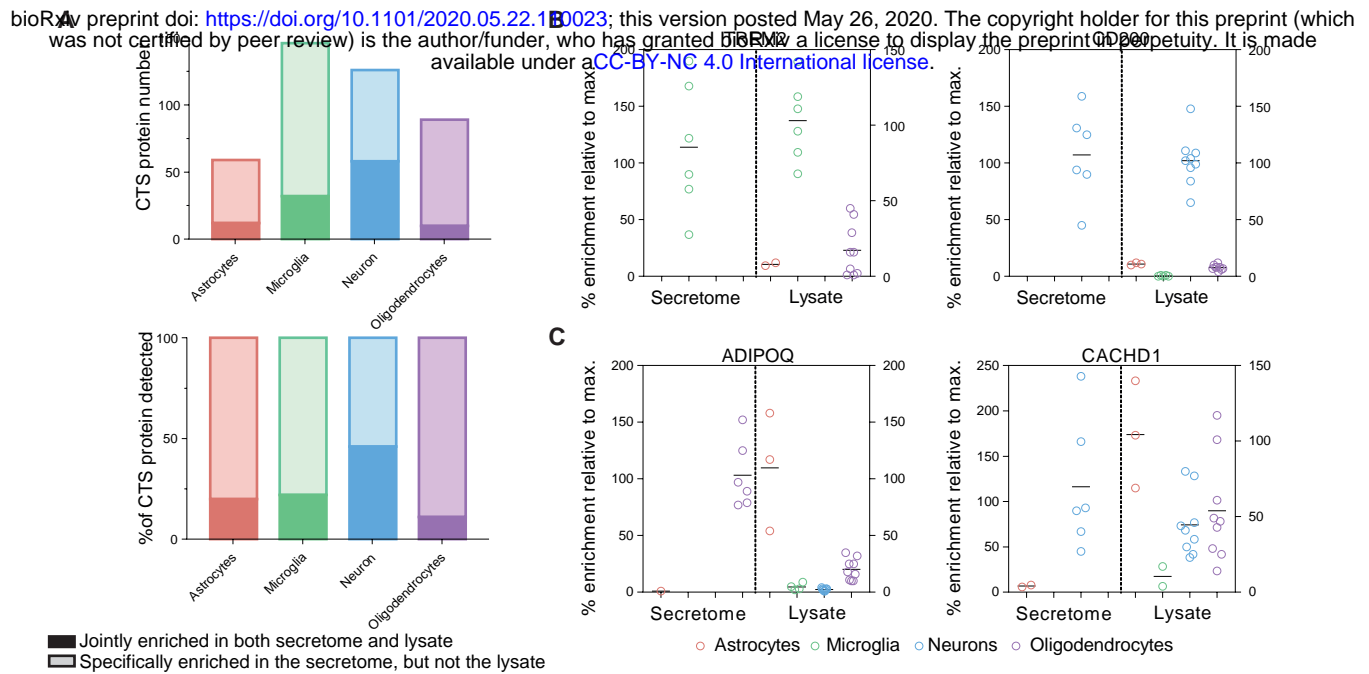


**Figure 5: Identification and validation of substrate candidates of the protease BACE1.**

bioRxiv preprint doi: <https://doi.org/10.1101/2020.05.22.110023>; this version posted May 26, 2020. The copyright holder for this preprint (which was not certified by peer review) is the author/funder, who has granted bioRxiv a license to display the preprint in perpetuity. It is made available under aCC-BY-NC 4.0 International license.

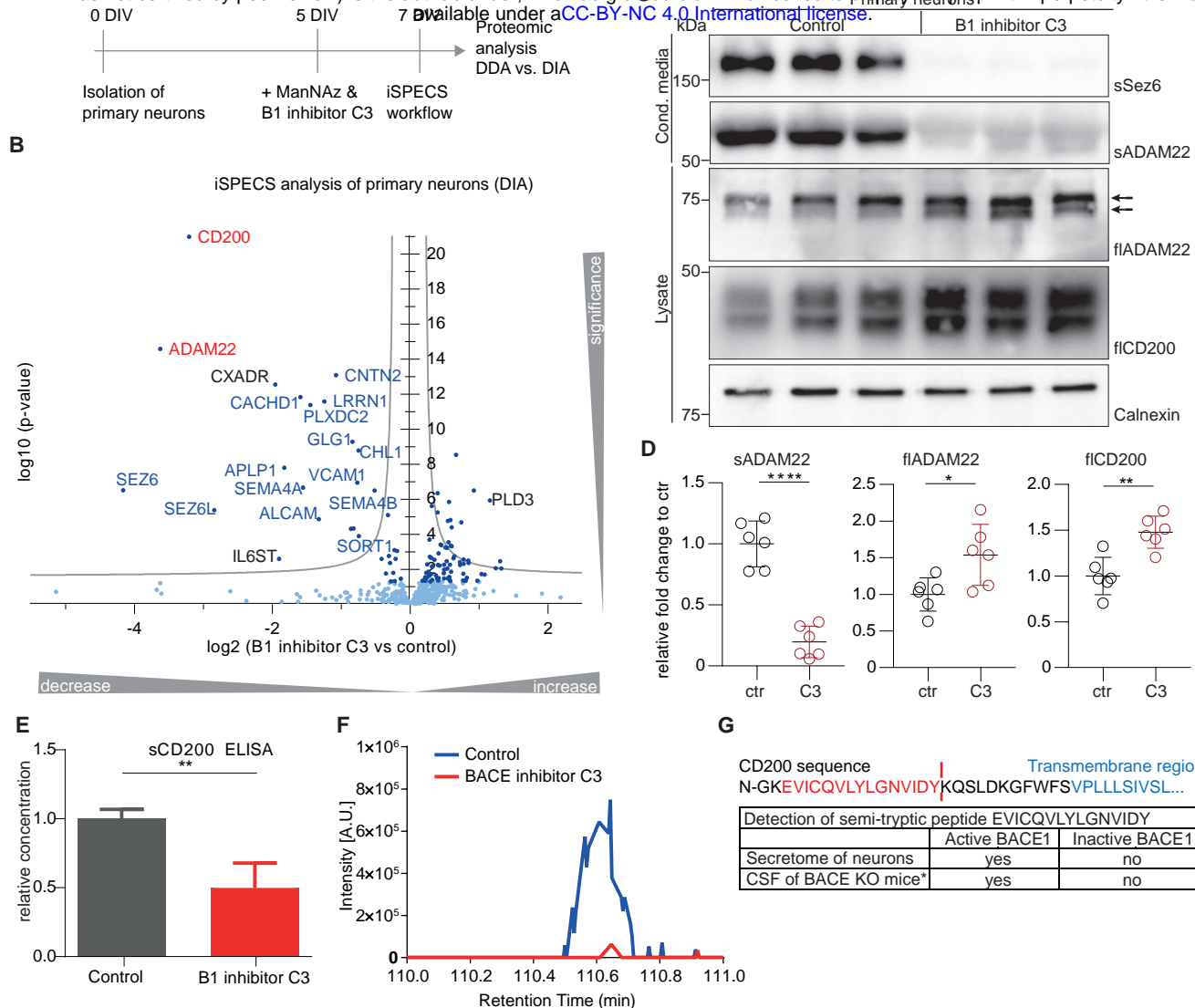


**Figure 6: Mapping of murine CSF proteins to their probable cell type origin.**

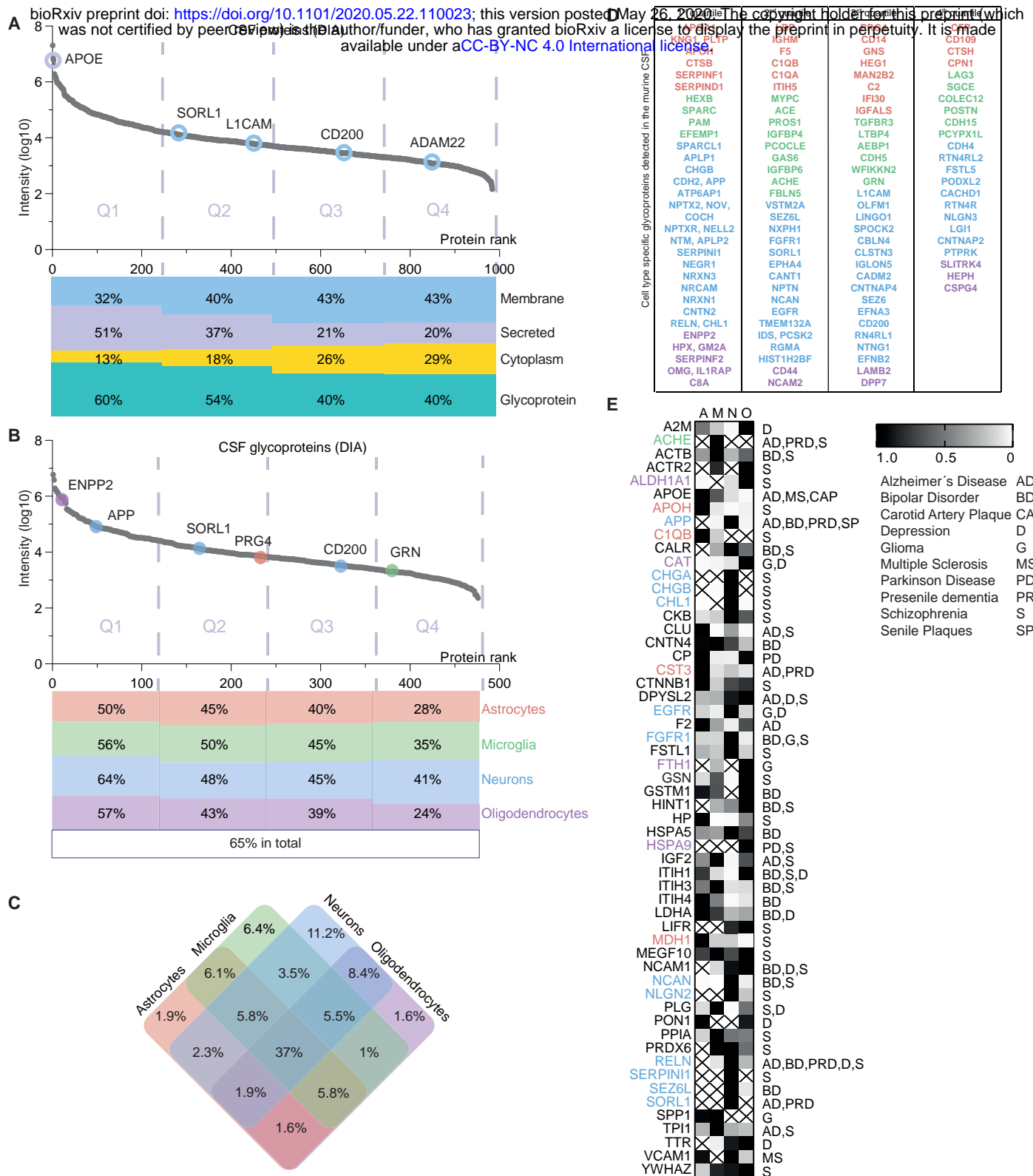
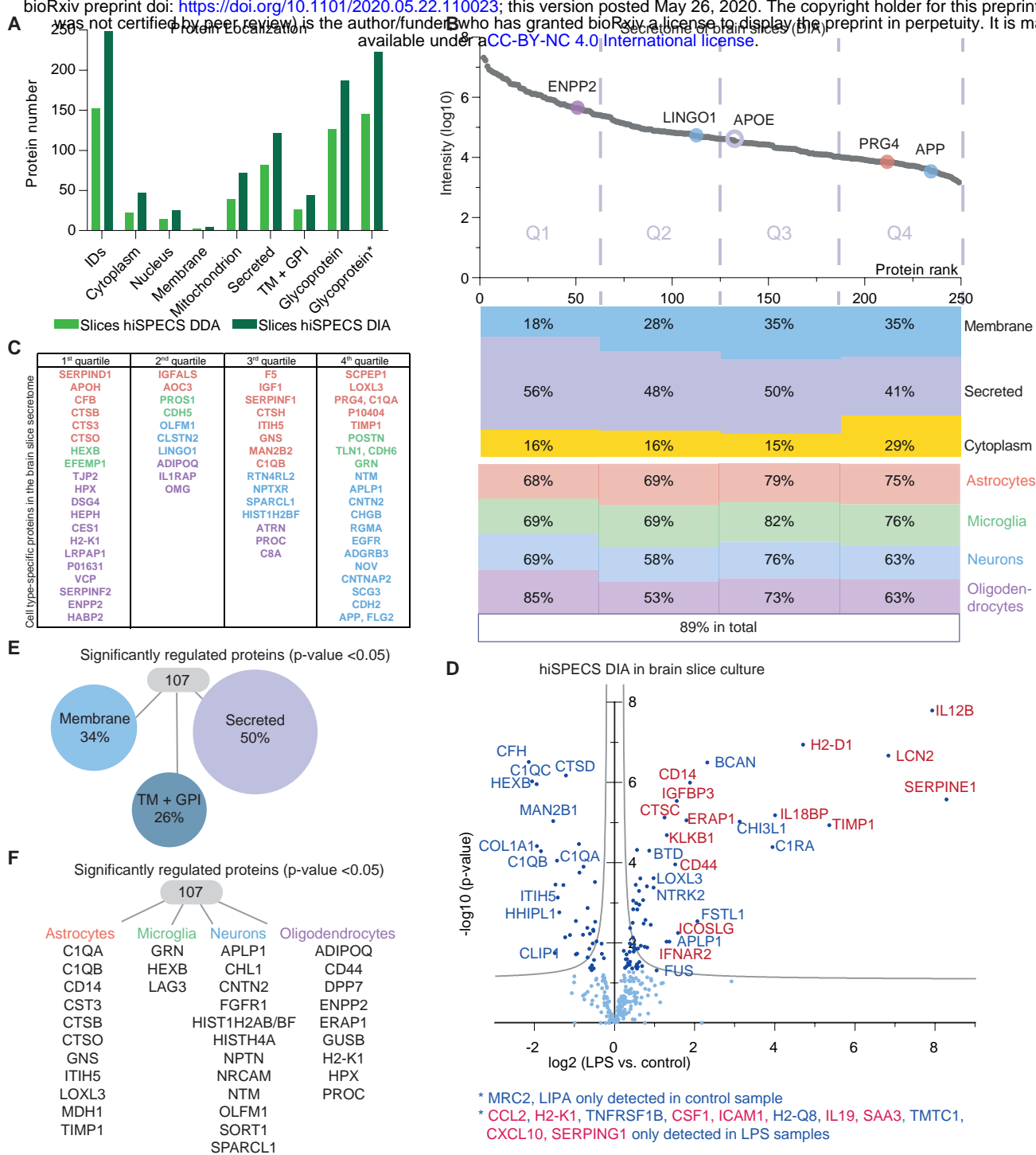


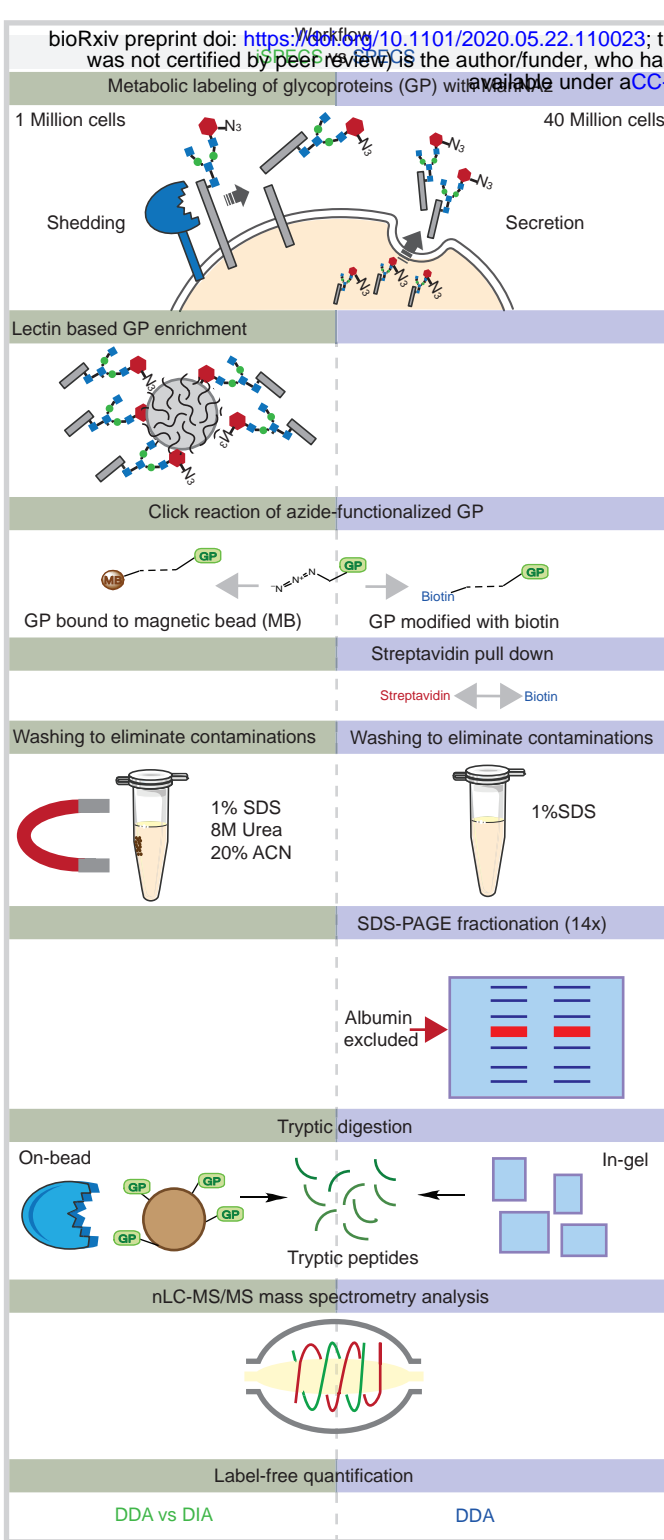
Figure 7: The secretome of brain slices.

bioRxiv preprint doi: <https://doi.org/10.1101/2020.05.22.110023>; this version posted May 26, 2020. The copyright holder for this preprint (which was not certified by peer review) is the author/funder, who has granted bioRxiv a license to display the preprint in perpetuity. It is made available under aCC-BY-NC 4.0 International license.

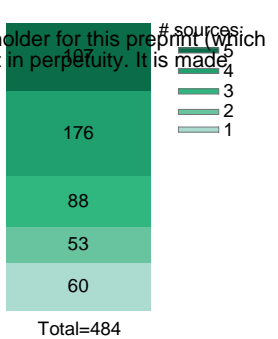
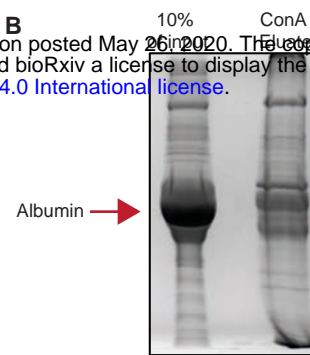


## Supplementary Fig.1: Benchmarking hiSPECS against SPECS.

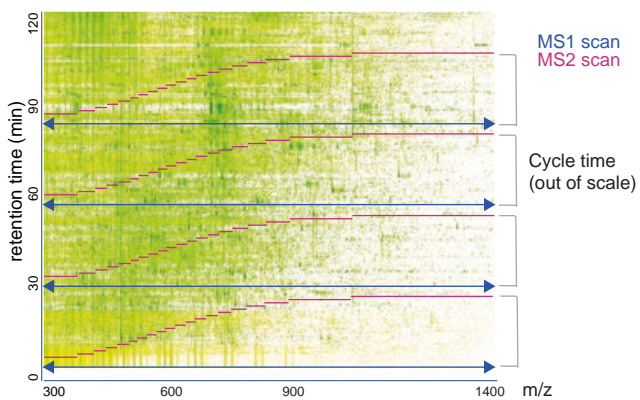
A



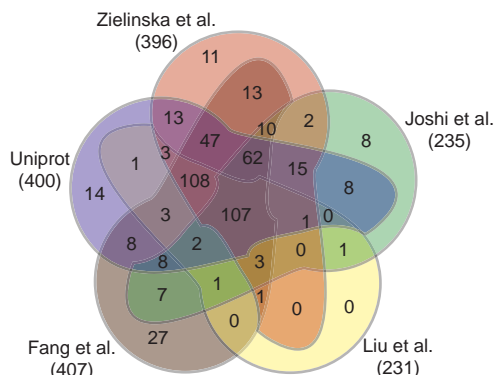
B



C



E

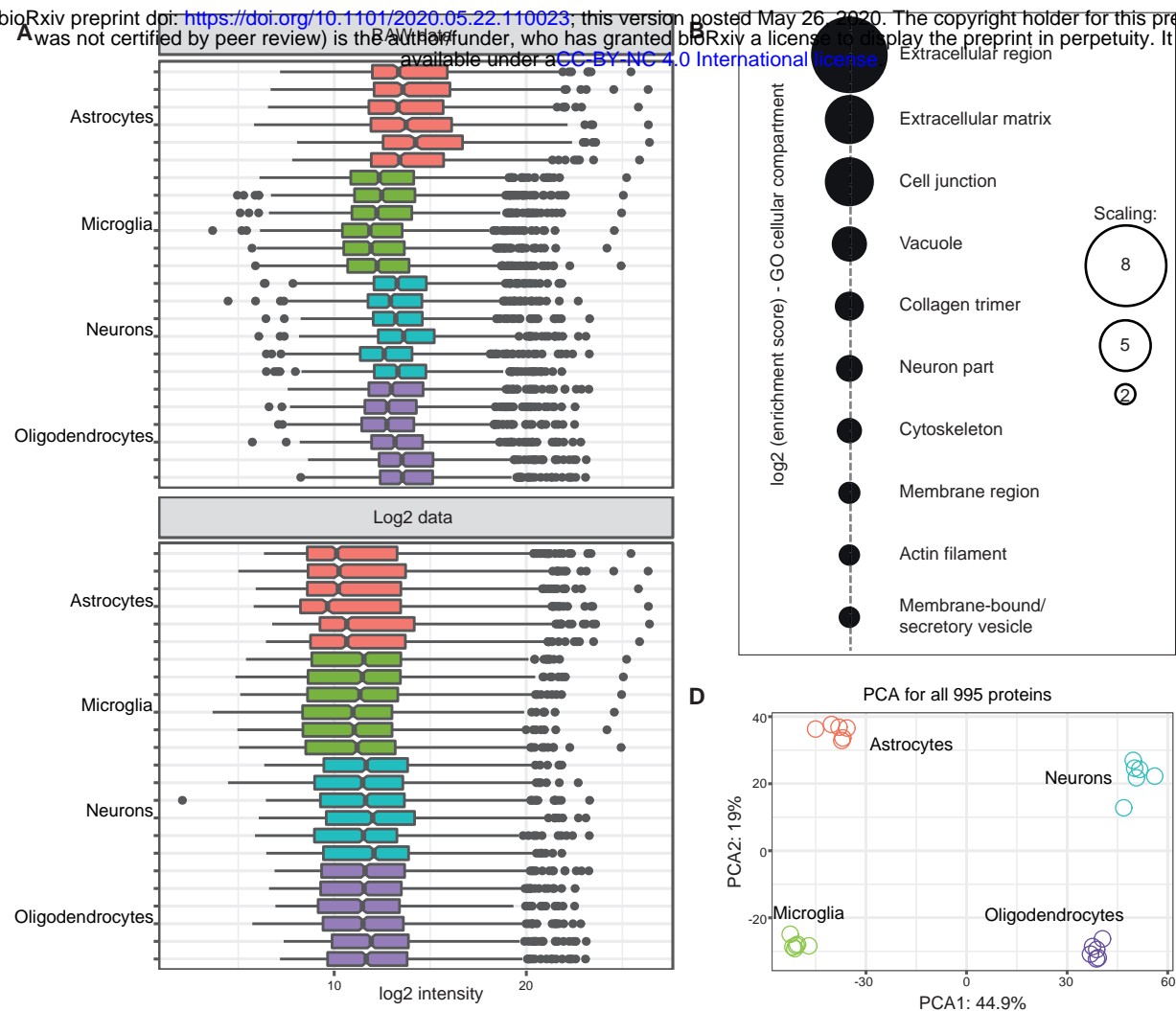


F

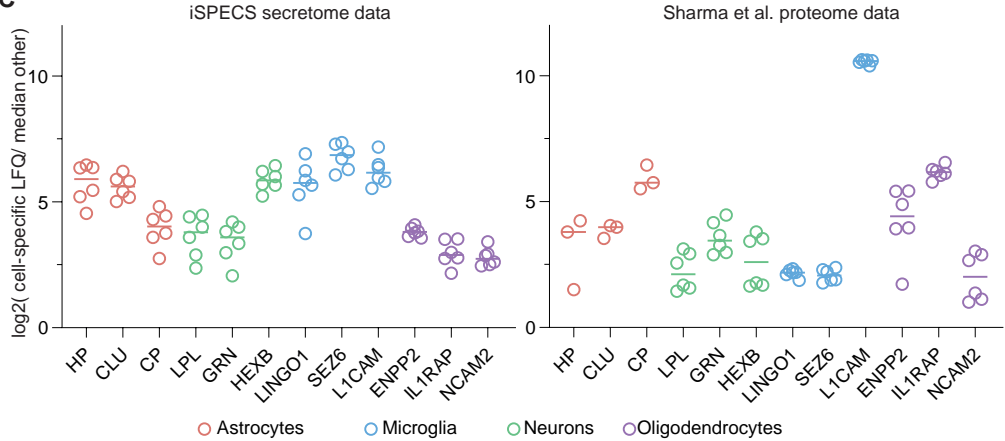


## Supplementary Figure 2: Quality control of cell type-resolved mouse brain glyco-secretome resource

bioRxiv preprint doi: <https://doi.org/10.1101/2020.05.22.110023>; this version posted May 26, 2020. The copyright holder for this preprint (which was not certified by peer review) is the author/funder, who has granted bioRxiv a license to display the preprint in perpetuity. It is made available under aCC-BY-NC 4.0 International license.

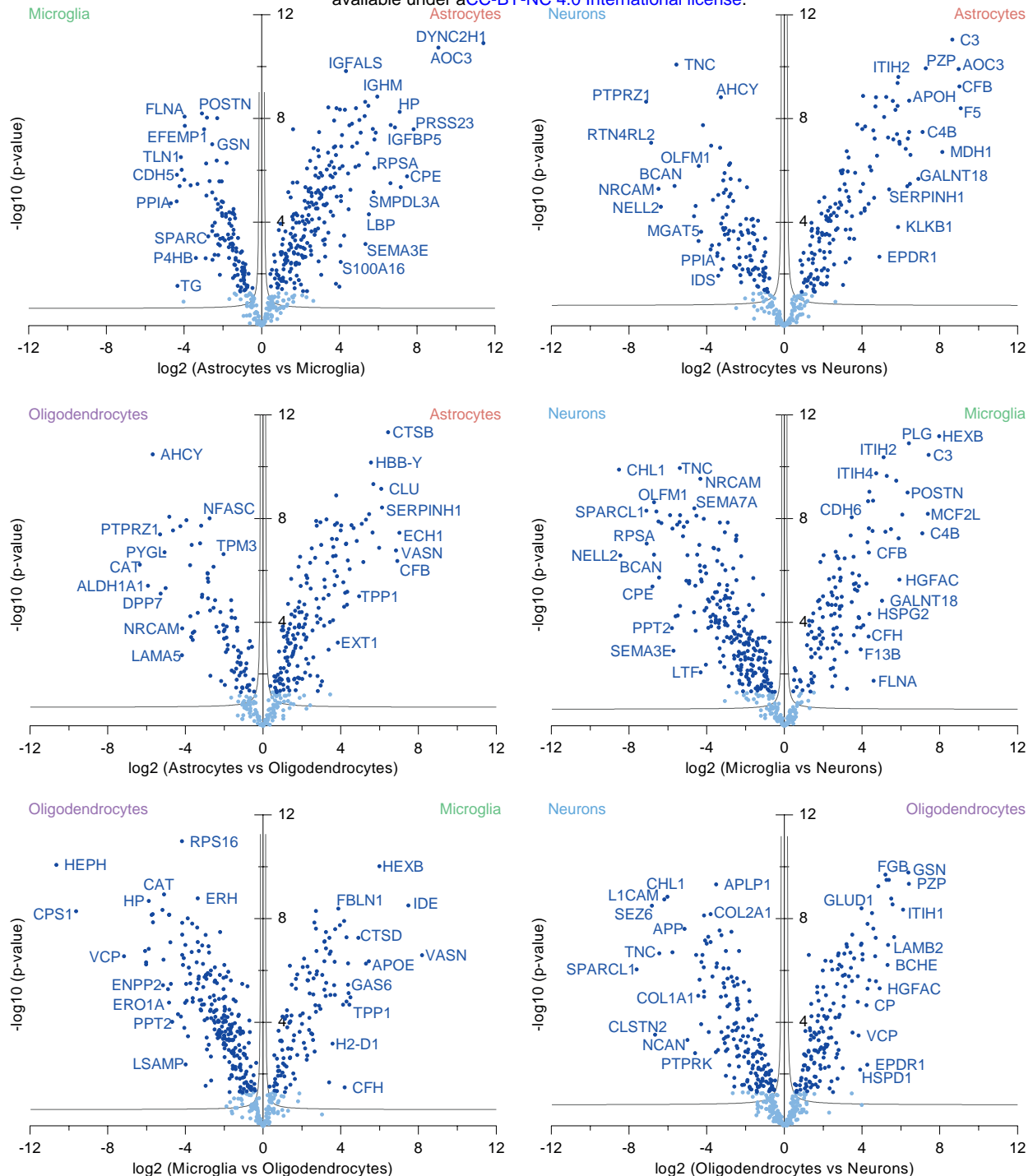


**C**



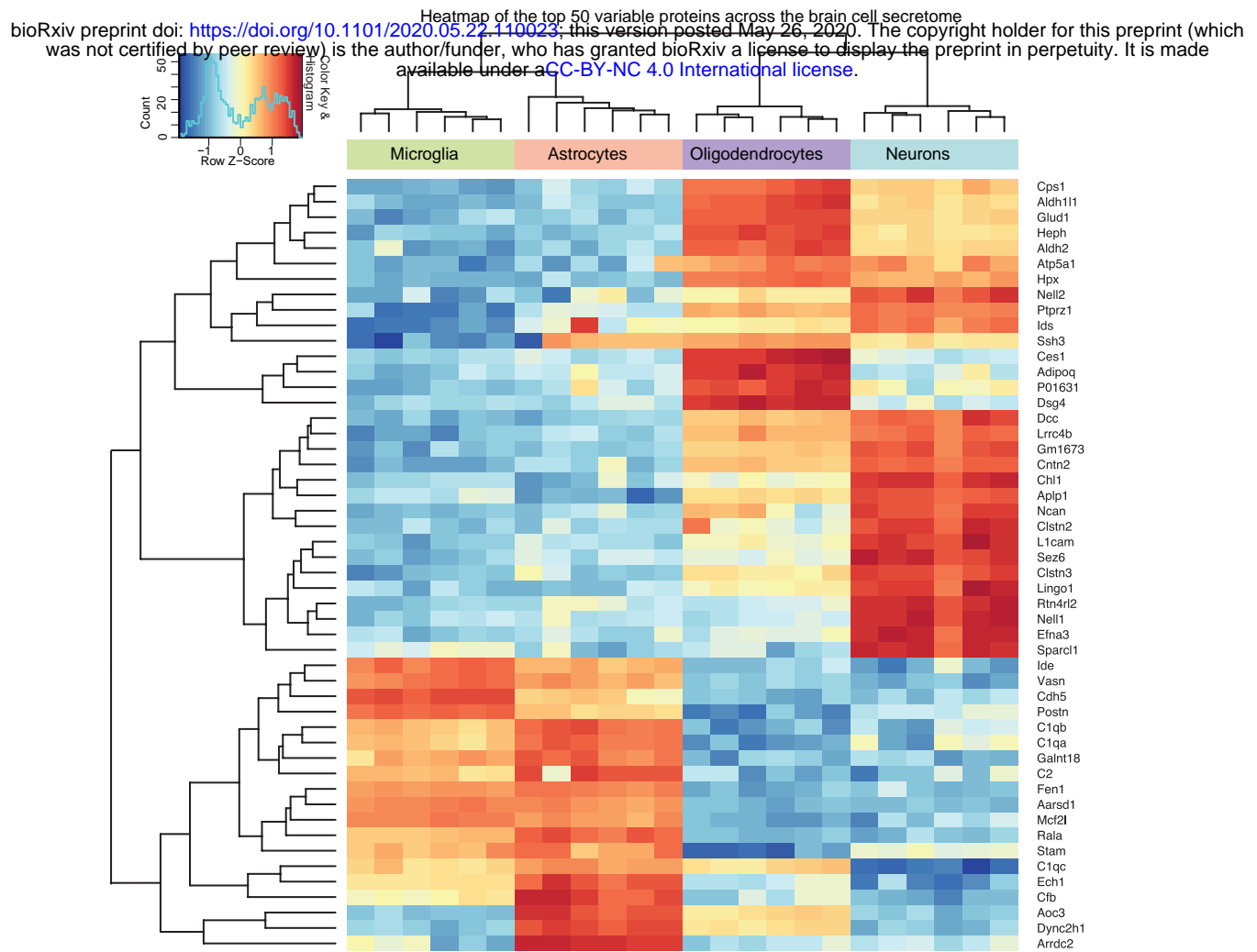
### Supplementary Figure 3: Diversity of cell type-resolved mouse brain glyco-secretome resource

bioRxiv preprint doi: <https://doi.org/10.1101/2020.05.22.110023>; this version posted May 26, 2020. The copyright holder for this preprint (which was not certified by peer review) is the author/funder, who has granted bioRxiv a license to display the preprint in perpetuity. It is made available under aCC-BY-NC 4.0 International license.

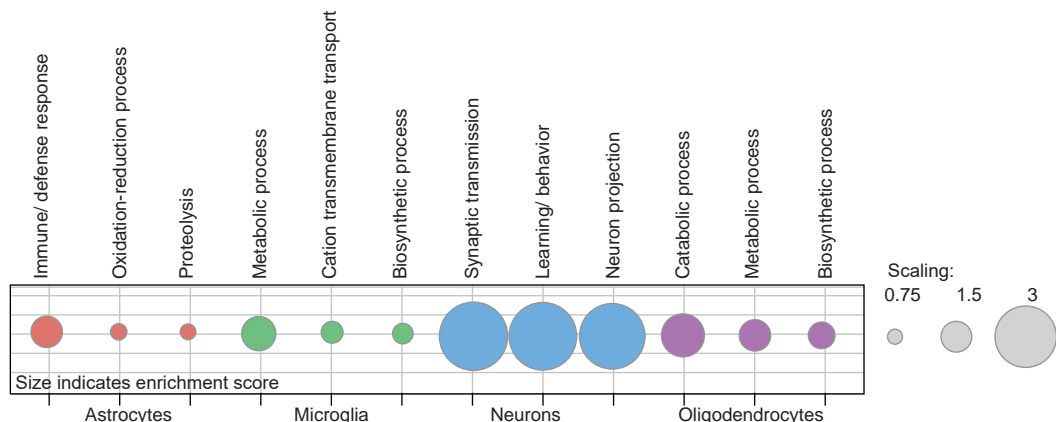


### Supplementary Figure 4: Top 50 cell type-specifically enriched proteins in the glyco-secretome resource.

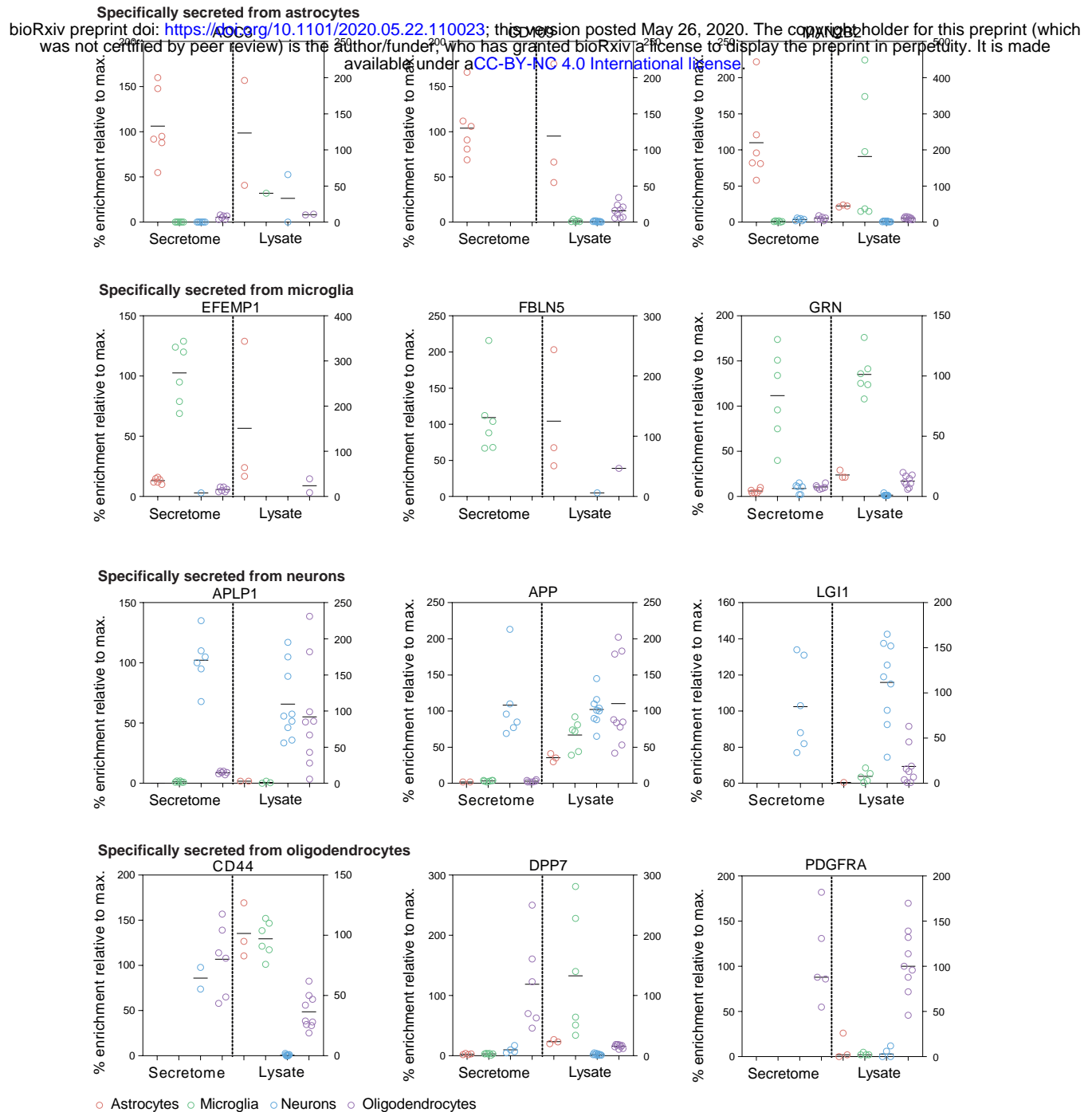
A



B

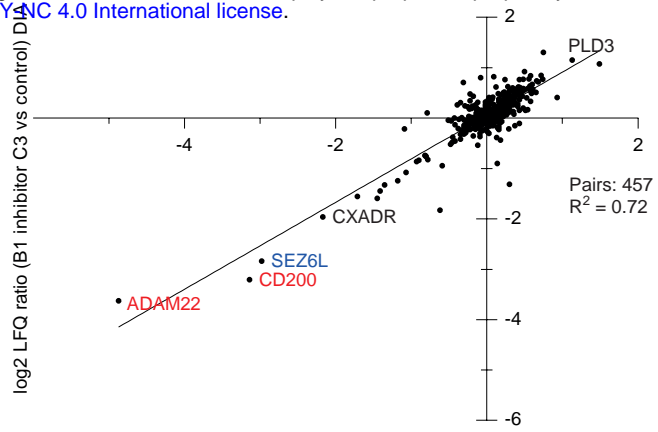
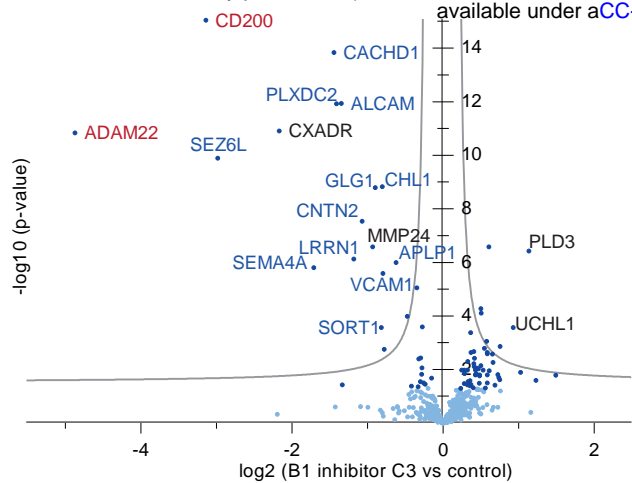


## Supplementary Figure 5: Protein levels in the brain cell secretome vs. lysate proteome.



**Supplementary Figure 6: Substrate candidate identification of the Alzheimer's protease BACE1 as proof of principle of the iSPECS method.**

bioRxiv preprint doi: <https://doi.org/10.1101/2020.05.22.110023>; this version posted May 26, 2020. The copyright holder for this preprint (which was not certified by peer review) is the author/funder, who has granted bioRxiv a license to display the preprint in perpetuity. It is made available under aCC-BY-NC 4.0 International license.



### Supplementary Figure 7: Top25 enriched proteins in the secretome of astrocytes, microglia, neurons and oligodendrocytes.

bioRxiv preprint doi: <https://doi.org/10.1101/2020.05.22.110023>; this version posted May 26, 2020. The copyright holder for this preprint (which was not certified by peer review) is the author/funder, who has granted bioRxiv a license to display the preprint in perpetuity. It is made available under aCC-BY-NC 4.0 International license.

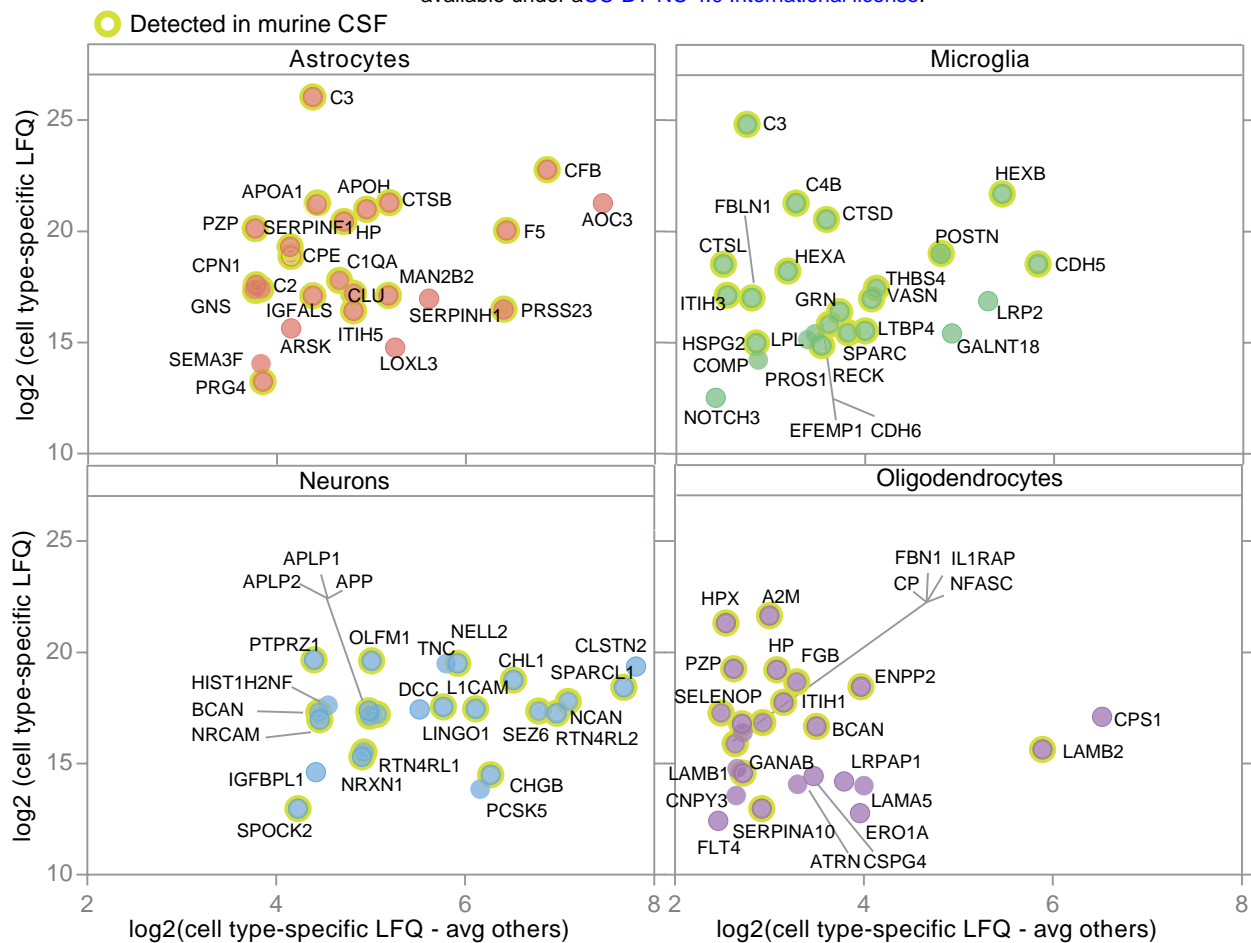


**Table S7: List of BACE1 substrate candidates.**

Summary of the significantly reduced proteins (p-values < 0.05) in the secretome of neurons upon pharmacological inhibition of BACE1 with C3 identified by the hiSPECS DIA method (Figure 4b). Listed are the gene names, UniProt accession, ratio between C3 vs control samples (DMSO), p-value and the topology of the proteins. Other proteomic studies are highlighted which previously showed a reduction of the proteins upon BACE1 inhibition in primary neurons or murine CSF.

Gene Name	UniProt Ac.	T-test p-value	Ratio (C3/Ctr)	Topology	Publication
Sez6	Q7TSK2	3.04E-07	0.06	TM1	
Adam22	Q9R1V6	2.55E-15	0.08	TM1	Kuhn et al., 2012
Cd200	O54901	1.04E-21	0.11	TM1	
Sez6l	Q6P1D5	4.25E-06	0.14	TM1	Kuhn et al., 2012
Cxadr	P97792	2.83E-13	0.26	TM1	
Il6st	Q00560	2.54E-03	0.27	TM1	
Aplp1	Q03157	1.60E-08	0.28	TM1	Kuhn et al., 2012; Zhou et al., 2012; Dislich et al., 2015
Cachd1	Q6PDJ1	1.46E-12	0.33	TM1	Kuhn et al., 2012
Sema4a	Q62178	2.17E-07	0.34	TM1	
Plxdc2	Q9DC11	4.07E-12	0.37	TM1	Kuhn et al., 2012; Zhou et al., 2012; Dislich et al., 2015
Alcam	Q61490	1.37E-05	0.40	TM1	
Lrrn1	Q61809	2.65E-12	0.42	TM1	Kuhn et al., 2012
Cntn2	Q61330	8.23E-14	0.47	GPI	Kuhn et al., 2012; Zhou et al., 2012; Dislich et al., 2015
Mmp24	Q9R0S2	4.96E-05	0.55	TM1	
Glg1	Q61543	5.19E-10	0.56	TM1	Kuhn et al., 2012,9
Fgfr1	P16092	4.61E-05	0.57	TM1	Kuhn et al., 2012; Zhou et al., 2012; Dislich et al., 2015
Vcam1	P29533	1.13E-07	0.59	TM1	
Chl1	P70232	1.64E-09	0.60	TM1	Kuhn et al., 2012; Zhou et al., 2012; Dislich et al., 2015
Sort1	Q6PHU5	1.25E-04	0.60	TM1	
Sema4b	Q62179	3.17E-07	0.70	TM1	Kuhn et al., 2012
Col4a1	P02463	2.50E-03	0.75		
Itm2b	O89051	1.77E-02	0.78	TM2	
Met	P16056	7.93E-06	0.80	TM1	
Col4a2	P08122	1.72E-03	0.81		
Robo1	O89026	4.41E-03	0.82	TM1	
Adam12	Q61824	4.85E-02	0.82	TM1	
Tyro3	P55144	5.02E-02	0.83	TM1	
Tnfrsf21	Q9EPU5	1.62E-02	0.84	TM1	
Sema6c	Q9WTM3	7.94E-04	0.85	TM1	
St6galnac 5	Q9QYJ1	4.80E-02	0.86	TM2	
Mdga1	Q0PMG2	2.57E-03	0.86	GPI	
Ptpg	Q05909	9.09E-04	0.88	TM1	
Rgma	Q6PCX7	3.51E-02	0.91	GPI	